Chapter 10
Soft Actuators

**Shingo Maeda, Yuhei Yamada, Hiroyuki Nabae, Kenjiro Tadakuma,
Koichi Suzumori, Zebing Mao, Jun Shintake, Hideyuki Sawada,
Yuya Morimoto, and Masahiro Shimizu**

Abstract We will discuss typical soft actuators in this chapter. In the overview, we showed that actuators are generally divided into equilibrium and non-equilibrium types in terms of energy dissipation and efficiency. We introduce the following categories of soft actuators: fluidic actuators, electroactive polymer actuators, thermomechanical actuators, and bioactuators. Furthermore, the types of actuators are summarized. Finally, we discuss the mechanical properties and performance of the various actuators.

S. Maeda (✉) · H. Nabae · K. Suzumori · Z. Mao
Department of Mechanical Engineering, Tokyo Institute of Technology, Tokyo, Japan
e-mail: maeda.s.ao@m.titech.ac.jp

H. Nabae
e-mail: nabae.h.aa@m.titech.ac.jp

K. Suzumori
e-mail: suzumori.k.aa@m.titech.ac.jp

Z. Mao
e-mail: mao.z.aa@m.titech.ac.jp

S. Maeda · Y. Yamada · K. Suzumori
Living Systems Materialogy (LiSM) Research Group, International Research Frontiers Initiative (IRFI), Tokyo Institute of Technology, Yokohama, Japan
e-mail: yamada.y.bw@m.titech.ac.jp

K. Tadakuma
Tohoku University, Sendai, Japan
e-mail: tadakuma@rm.is.tohoku.ac.jp

J. Shintake
Department of Mechanical and Intelligent Systems Engineering, The University of Electro-Communications, Chōfu, Japan
e-mail: shintake@uec.ac.jp

H. Sawada
Department of Applied Physics, Faculty of Science and Engineering, Waseda University, Tokyo, Japan
e-mail: sawada@waseda.jp

10.1 Overview

10.1.1 Introduction

An actuator is a device that controls the mechanical movement of a machine system. The word "actuator" is often used ambiguously. In this chapter, we define an actuator as any device that converts energy into mechanical energy. Unlike conventional actuators that are usually hard in the sense of the material and control mechanism, actuators with a soft body or fuzzy controllability are called soft actuators. Herein, we introduce a mathematical framework for actuators and discuss the meaning and role of "softness."

10.1.2 Mathematical Framework

We consider an actuator as "a system whose state at a given time is uniquely determined by a set of variables and that exerts a force on the outside through deformation." For simplicity, let us denote the variable that characterizes the shape of the actuator as x (which corresponds to the length if it is a piston-type actuator) and the variable that characterizes the force that balances the external load as f. We then consider a one-dimensional motion in which the direction of deformation and that of the force are parallel. Note that generalization of the discussion to a multidimensional case or transformation of variables to corresponding ones is straightforward.

When the state of the actuator is fully specified by x, f, and n variables $\boldsymbol{\theta} = (\theta_1, \theta_2, \ldots, \theta_n)$ that characterize the internal state, the variables are related by a function Φ as

$$f = \Phi(x, \boldsymbol{\theta}) \tag{10.1}$$

We refer to Eq. (10.1) as the equation of state of the actuator, and we denote the state of the actuator at time t as $(f, x, \boldsymbol{\theta}; t)$ (Fig. 10.1).[1]

Y. Morimoto
Department of Mechano-Informatics, Graduate School of Information Science and Technology, The University of Tokyo, Tokyo, Japan
e-mail: y-morimo@hybrid.t.u-tokyo.ac.jp

M. Shimizu
Department of Systems Innovation, Graduate School of Engineering Science, Osaka University, Toyonaka, Japan
e-mail: m_shimizu@nagahama-i-bio.ac.jp

[1] When we replace f with pressure P, x with volume V, and θ with temperature T, Eq. (10.1) corresponds to the thermodynamic equation of state. However, the variables here do not necessarily have to be thermodynamic variables; we can say that Eq. (10.1) is a generalized equation of the thermodynamic equation of state. Although this formulation apparently ignores the effect of hysteresis,

Fig. 10.1 Schematic of an
actuator
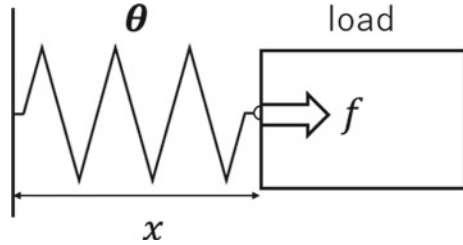
10.1.3 Energy and Work

Actuators are often designed to work repetitively through cyclic operations. In this
case, it is convenient to define efficiency as the ratio of the energy required to change
the state of an actuator to the work output for a cycle. Suppose that, during time Δt,
the state of the actuator changes by Δf, Δx, and $\Delta \boldsymbol{\theta}$. We denote the energy required
to cause the change as

$$dE[(f, x, \theta; t) \rightarrow (f + \Delta f, x + \Delta x, \boldsymbol{\theta} + \Delta \boldsymbol{\theta}; t + \Delta t)] \tag{10.2}$$

By repeating the change, we can define a sequential process that returns to its
original state. We refer to the sequential process as a cycle and denote it by C. The
energy required to realize the cycle can be expressed as

$$E = \oint_C dE \tag{10.3}$$

We can calculate f and dx, the displacement of x, for each small change in the
state. Integrating the product of f and dx over a cycle, we obtain the work output W
as

$$W = \oint_C f \, dx \tag{10.4}$$

The efficiency of the actuator for a cycle C is then defined as

$$\eta_C = \frac{W}{E} \tag{10.5}$$

Depending on the nature of dE, we can divide actuators into two types. Consider
the process of time Δt maintaining its state. When the energy required for the process
is zero, i.e.,

---

the effect can be discussed within the same framework if we can add variables that characterize the
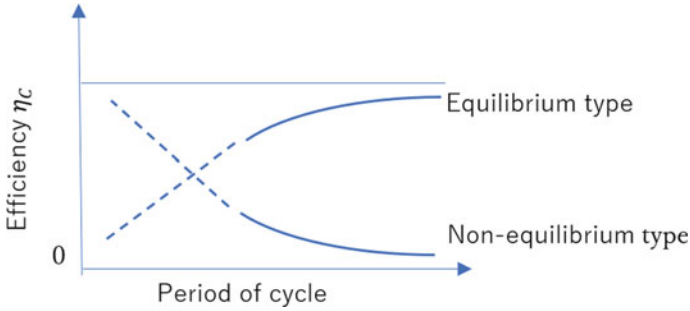effect as $\boldsymbol{\theta}$.

Fig. 10.2 Schematic of the relationship between efficiency and time for equilibrium- and non-equilibrium-type actuators

$$\mathrm{d}E[(f, x, \boldsymbol{\theta}; t) \rightarrow (f, x, \boldsymbol{\theta}; t + \Delta t)] = 0 \qquad (10.6)$$

the actuator is classified as an "equilibrium-type." Examples include heat engines, shape-memory alloys (SMAs), piezo actuators, and dielectric elastomer actuators (DEAs). However, when the energy required for the process is not zero, i.e.,

$$\mathrm{d}E[(f, x, \boldsymbol{\theta}; t) \rightarrow (f, x, \boldsymbol{\theta}; t + \Delta t)] \neq 0 \qquad (10.7)$$

the actuator is classified as a "non-equilibrium type." Examples include actuators that use electromagnetic motors and fluid pumps. The relationship between operation time and efficiency of actuators exhibits contrasting behaviors depending on the type. Because the dissipation of an equilibrium-type actuator becomes smaller with increasing Δt, E becomes the minimum at the limit of $\Delta t \rightarrow \infty$, which corresponds to the quasi-static process of thermodynamics. Subsequently, the η_C becomes maximum when the cycle is composed of the quasi-static process. However, in a non-equilibrium-type actuator, both the dissipation and E increase with increasing Δt because energy dissipation occurs constantly. Then, E becomes infinitely large and η_C becomes zero when the cycle is composed of the quasi-static process. In practical use, we can utilize some mechanisms such as valves for a non-equilibrium-type actuator to avoid energy consumption and maintain its state. We can then prevent the decrease in efficiency by increasing the time of a cycle (Fig. 10.2).

10.1.4 "Softness" of the Actuator

One of the characteristics of soft actuators is that they are composed of soft materials. Softness physically means that a large deformation is induced by a small force. When a tensile or compressive force is applied to an object, the stress–strain relationship between the "hard" and "soft" objects is typically represented as shown in Fig. 10.3. What effect does this softness have on the performance of actuators? As a typical

Fig. 10.3 Stress–strain
relationship for hard and soft
actuators
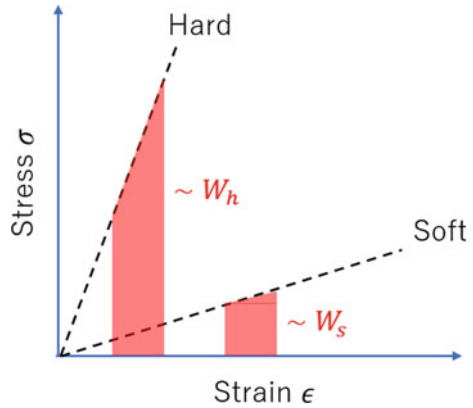
example, consider a one-stroke process of a piston-type actuator in which the control
variable $\boldsymbol{\theta}$ is functionally switched stepwise from $\boldsymbol{\theta}_0$ to $\boldsymbol{\theta}_1$ at $t = 0$ and in which
work is produced by quasi-static changes in x and f. Suppose that x increases
monotonically during this process and $f \geq 0$. Additionally, suppose that x varies
from x_0 to x_1 and that f varies from f_0 to f_1. The relationship between x and f during
this process is expressed using the equation-of-state Eq. (10.1) as $\boldsymbol{\theta} = \boldsymbol{\theta}_1$:

$$f = \Phi(x, \boldsymbol{\theta}_1) \tag{10.8}$$

We now define the strain as

$$\epsilon = \frac{x_1 - x}{x_1} \tag{10.9}$$

and the stress σ is defined as the amount of f divided by the cross-sectional area A
on which the force acts. The relationship between ϵ and σ then corresponds to the
stress–strain relationship obtained from mechanical measurements when $\boldsymbol{\theta} = \boldsymbol{\theta}_1$.
The work output of the process is equal to the integral of the stress–strain curve with
the change in strain multiplied by $A \times x_1$. As shown in Fig. 10.3, compared with
hard actuators, soft actuators usually encounter greater difficulty generating large
forces, and the work produced by a soft actuator W_s tends to be smaller than that
produced by a hard actuator W_h. However, when adaptability to the environment is
considered, soft actuators are often more capable than hard actuators. Because soft
actuators are deformable, they offer the advantage of allowing a certain degree of
freedom in selecting the load. By defining the input energy as E_{in}, work output as
W', and energy required for deformation as E_d, we can express the relationship as

$$E_{in} = W' + E_d \tag{10.10}$$

Here, we ignore the dissipated energy. Because hard actuators are difficult to
deform, E_d becomes smaller than W' and the opposite takes place for soft actuators.

Fig. 10.4 Simple model of a soft actuator (and work object) using linear spring elements
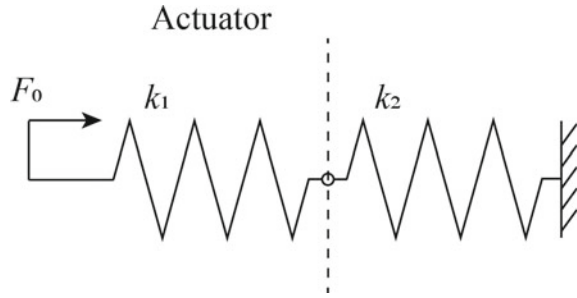
Let us consider the energy distribution through a simple model in which the actuator and load are modeled using linear springs (Fig. 10.4). Parameters k_1 and k_2 are the spring constants of the actuator and load, respectively, and F_0 denotes the input force to the actuator. For example, in the case of a pneumatic actuator, this input corresponds to the force (or pressure) exerted by a pump and the elasticity represents the mechanical property of a composite composed of air and the actuator's body. Consider the energy E_d used to deform the actuator and the work W' performed on the load. The displacement of the actuator is F_0/k_1 and that of the load is F_0/k_2. Then, E_d and W' become

$$E_d = \frac{F_0^2}{2k_1} \tag{10.11}$$

$$W' = \frac{F_0^2}{2k_2} \tag{10.12}$$

In the case of soft actuators, $k_1 < k_2$ and then $E_d > W'$, as previously discussed. The present example is an extremely idealized model used to discuss the interaction between the actuator and load. In practical cases, we need to consider nonlinearities of elasticity to evaluate the energies, especially those for soft actuators, because they often exhibit large deformations in their operation. Moreover, other characteristics of the actuator, load, and interacting environment also affect the energy distribution. Such individual cases should be treated separately.

Finally, the discussion here is just a brief comparison of the softness of actuators.[2] Hard and soft actuators should not be treated as superior or inferior; they are complementary concepts. Both types of actuators are needed depending on the situation.

---

[2] We are discussing a typical case here; however, methods such as "soft-rigid switching," in which the stiffness is temporarily changed to increase the work output W', have also been proposed for soft actuators.

10.1.5 Types and Classification of Actuators

In this section, we focus on (1) the physical process of extracting work and (2) the state of the working material and describe the characteristics of each of these. Although there are various viewpoints for classifying actuators, we classify actuators for extracting motion into five major types: thermodynamic type, light type, mechanical type, electromagnetic type, and bio-type. We classified each type by the index of the control parameter and driving principle and organized the entire classification. The thermodynamic, light, mechanical, electromagnetic, and bio types correspond to the physical phenomena that govern each type.

Thermal actuators, SMAs/shape-memory polymers (SMPs) (Higuchi et al. 2009), and thermoresponsive gel actuators (Yeghiazarian et al. 2005) are typical examples of thermodynamic-type actuators. The fishing-line artificial muscle (Haines et al. 2014) is a thermal-type actuator. By fabricating the fiber structure in the form of a coil, researchers have achieved large expansion and contraction.

Piezoelectric actuators (Higuchi et al. 2009), DEAs (Ji et al. 2019), IPMC actuators (Kodaira et al. 2019), polyvinyl chloride (PVC) gel actuators (Li and Hashimoto 2016), and EHD actuators (Cacucciolo et al. 2019) are examples of electromagnetic-type actuators. There are several actuators whose control parameter is electric field (Table 10.1).

Importantly, the driving principles of actuators driven by electrostatic force, such as DEAs and HASELs, and those driven by ion conduction, such as IPMC actuators, differ fundamentally. In the field of artificial muscle research, electroactive polymers have been attracting attention as polymers that can be electrically driven (Cohen 2004).

Figure 10.5 shows the relationship among various actuators. Numerous graphs have been reported by many researchers. However, because the experimental conditions differ, the graphs are inconsistent. We therefore note that we created Fig. 10.5 intuitively. Herein, we used Huber et al. (1997) wherein the authors considered the process of one stroke, in which an actuator does work against a load. They defined actuation stress σ_a as the force divided by the cross-sectional area A on which the force acts and actuation strain ϵ_a as the displacement produced by the actuator divided by the original length L of the actuator.

10.1.6 Challenges

Throughout this section, we have discussed the characteristics of soft actuators. Although we have attempted to keep the discussion as general as possible, there are still some important issues that could not be addressed here. For example, the following issues were not discussed:

- How can we describe the efficiency in a non-steady state when considering the efficiency of equilibrium- and non-equilibrium-type actuators shown in Fig. 10.2?

Table 10.1 Classes of actuators

Type	Control parameter	Driving principle	Actuator
Thermodynamic type	Temperature	Entropic force	Thermal actuator
		Phase transition (solid)	SMA/SMP
		Phase transition (liquid–vapor)	Phase-change actuator/pouch motor
		Osmotic pressure	Gel actuator
	Concentration	Osmotic pressure	Gel actuator
		Equilibrium hydrogen pressure	Hydrogen storage alloy
Light type	Light	Photomechanical effect	Photomechanical actuator
		Photostrictive	Photostrictive actuator
Mechanical type	Pressure	Hydraulic pressure	Hydraulic actuator
		Air pressure	Pneumatic actuator
Electromagnetic type	Electric field	Piezoelectric effect	Piezoelectric actuator
		Electrostatic force	DEA
			HASEL
			ERF actuator
		Ion conduction	IPMC actuator
			Gel actuator
			Conducting polymer actuator
			PVC gel actuator
			EHD actuator
	Magnetic field	Magnetic force	Electromagnetic actuator
			MR fluid actuator
Bio type	Concentration	Molecular machine[3]	Bioactuator

- How can we calculate the work that the actuator can do on the object under a load? How can we calculate the efficiency in such a situation?
- What happens if the system shown in Fig. 10.4 is a nonlinear one? How can we generalize the actuator and the load?
- How can we understand the cycle of the actuator in finite time and dissipation in the actuator?

Here, we provide additional explanations of these issues. First, although we omitted the discussion of finite-time operation of actuators, it is a critical issue in

---

[3] Biological system is quite complex, and there are still many concepts about various mechanisms in living beings that are yet to be understood. Therefore, at present, it is quite difficult for us to state the driving principle of the bio-type actuators.

Fig. 10.5 Actuation stress–strain for actuators
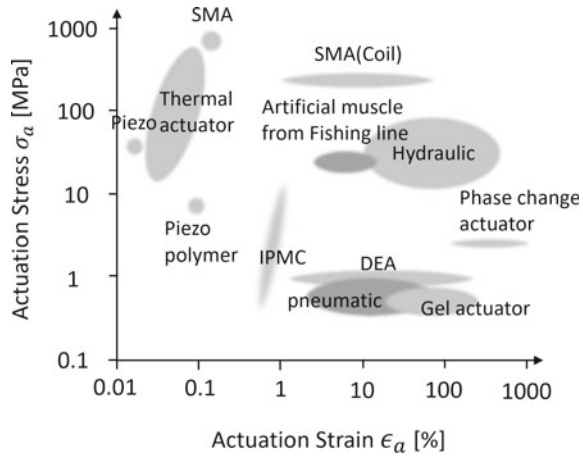
actual applications. In most cases, soft materials take longer to respond to mechanical forces than hard materials. For example, when considering the work production by a periodic signal input, soft actuators will have an upper operational frequency limit because of the limited deformation speed. To calculate the operational frequency limit, we must consider the material's viscosity. Another critical issue is the interaction of soft actuators with loads. As discussed in Sect. 10.1.3, the work output depends greatly on the nature of the load. Although the same issue arises in hard actuators, it is more serious in soft actuators because a greater amount of energy is used to deform soft materials. In practical applications, the choice of load (or the design and selection of the actuator) that maximizes the work output is an important issue for improving energy efficiency. We need to develop systematic theories for methods of matching loads and actuators depending on the nature of the materials. Moreover, it is important to consider energy dissipation in soft actuators. In soft materials, heat dissipation is often associated with deformation. Because large and fast deformations of the material induce greater dissipation, understanding and controlling dissipation is important for soft actuators.

10.2 Fluidic Actuators

10.2.1 Introduction

Conventional fluidic actuators or cylinders consist of a hollow cylinder with a piston inserted into them (Fig. 10.6a). Fluidic actuators acquire power from a pressurized working fluid such as fluidic oil. Structurally, fluidic actuators consist of a cylindrical barrel in which a piston rod can move back and forth. To seal the fluidic actuators, the piston usually comprises sliding seals and rings. A biased pressure provided by a

mechanical pump is applied to the piston, which can move an external load. In the case of a single action, the piston can move unidirectionally when fluid pressure is applied to one side of the piston. A spring is then used to provide the piston a return stroke for a single-acting cylinder. As a force difference exists between the two sides of the piston, the piston can move from one side to the other. The fluidic actuators can precisely control the linear displacement of the piston when incompressible fluid is used as the working fluid. Conventional fluidic actuators are extensively used in numerous applications (e.g., excavators, vehicles, drilling rigs, and conveyors). Compared with their rigid counterparts, fluidic elastomer actuators (FEAs) are a new type of highly extensible, adaptable, low-power soft actuators that are flexible, resilient to perturbations, and safe for human–robot interactions (Fig. 10.6b). The fluidic actuation can be used to inflate the elastomer chamber and induce the desired deformation. Therefore, fluidic actuators are typically fabricated from advanced organic elastomers and are operated by the deformation of the chamber or embedded channels by pressurized fluids. These organic elastomers, which are readily available from commercial vendors (e.g., Dow-Corning and Shin-Etsu), have low hysteresis and high flexibility with low elastic moduli. Stress–strain curves of these elastomers are used to evaluate their suitability. The slope of the curves reveals some of the elastomers' properties, including their elastic modulus (E) and toughness (G). Therefore, the soft fluidic actuators rely on pressurization due to the used properties of the intrinsic materials (Polygerinos et al. 2017). FEAs operate pneumatically or hydraulically because fluids are advantageous for generating large forces at the expense of increased weight and viscosity.

Various FEAs have emerged since the earliest research in 1989 by Suzumori et al. (1992). They can be roughly classified into four types on the basis of their locomotion: expanding, contracting, twisting, and bending (Fig. 10.7). Fluidic actuators can
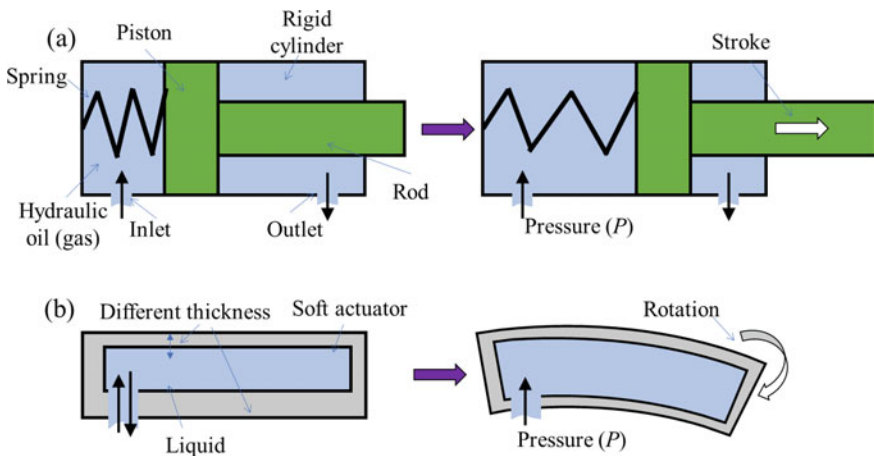

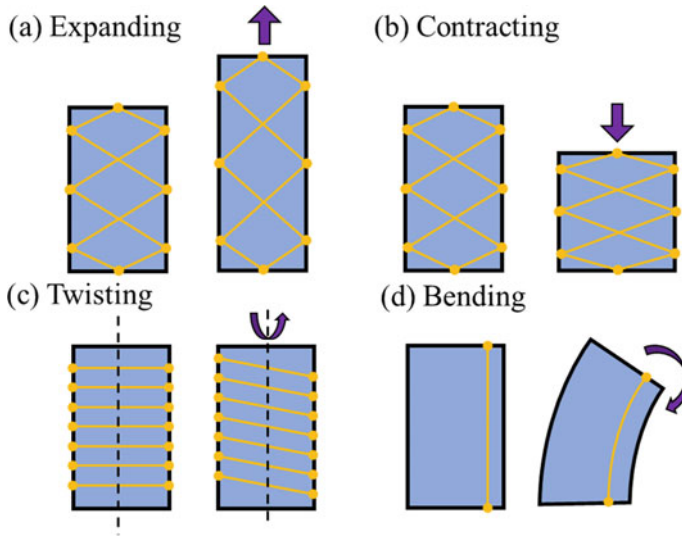**Fig. 10.6** **a** Conventional and **b** soft fluidic actuators

Fig. 10.7 Categories of fluidic actuators according to their deformation: **a** expanding, **b** contracting, **c** twisting, and **d** bending

be inflated by a pressurized fluid because of their carefully designed flexible structures. The structures of expanding and contracting actuators typically have symmetrical cross-sections; linear motion is induced as the fluid pressure is transmitted to the inner chamber. The famous contracting motion of McKibben actuators can be achieved using strain-limiting fibers (Hiramitsu et al. 2019). In twisting actuators, asymmetric structures composed of spiraling fibers can generate twisting motions. In the case of bending actuators, the design of the fluidic actuators is often asymmetrical, which enables deflection when a liquid is pressurized. When sophisticated fluidic actuators are studied, their motion path can be divided into one or more of the four aforementioned elements. Interesting or targeted motions such as gripping, rolling, quadrupedal locomotion, grasping, jumping, and snake-like undulation can be achieved via a combination of the four elements (Gorissen et al. 2017).

10.2.2   Fundamentals, Design, and Modeling

1.   Fundamentals

Pressure (p or P) and flow rate (q or Q) are often used to evaluate the power driving a fluidic actuator. Pressure is defined as the force applied perpendicular to the surface of an object per unit area, which obeys Pascal's law (Elger et al. 2020). According to this law, when an external pressure is applied to an incompressible liquid, it is transmitted equally throughout the liquid (Fig. 10.8a). The SI unit of pressure is
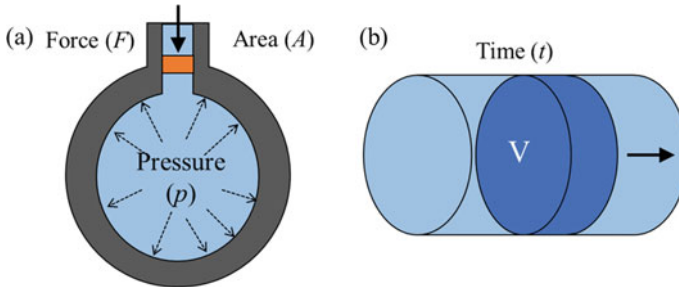
Fig. 10.8 Schematics demonstrating **a** Pascal's law and **b** the volumetric flow rate

pascal (Pa), which is defined as one newton per square meter (N/m^2). Pressure is calculated using

$$p = \frac{F}{A} \tag{10.13}$$

where p, F, and A are the pressure, the magnitude of the force, and the area of the contact surface, respectively. Fluid pressure, which often refers to the compressive stress at some point in a fluid, can be divided into two categories: open-channel flow (e.g., the ocean/atmosphere) or closed-conduit flow (e.g., a closed chamber). Soft fluidic actuators belong to the closed-conduit type. In the closed body of the soft liquid actuators, the fluid is either "static" or "dynamic." When the fluid is not moving, the pressure at any given point is referred to as the hydrostatic pressure. The following Bernoulli equation is used to determine the pressure at any point in a fluid. The underlying assumption is that the ideal and incompressible fluid is inviscid (i.e., lacks viscosity). Note that ρ, g, v, and z are density, acceleration of gravity, velocity of the fluid, and elevation, respectively.

$$\frac{p}{\rho g} + \frac{v^2}{2g} + z = \text{const.} \tag{10.14}$$

The flow rate is known as the volumetric flow rate, which is defined as the volume of fluid per unit time (Fig. 10.8b). The SI unit of volumetric flow rate is cubic meters per second (m^3/s). The change in volume is the amount of liquid that flows through the boundary within a given period. Therefore, the volumetric flow rate is defined as

$$Q = \frac{dV}{dt} \tag{10.15}$$

where V, Q, and t are the liquid volume, flow rate, and time, respectively. This volumetric flow rate is a scalar quantity because it is the time derivative of the volume and not the difference between the final and initial volumes at the boundary. To calculate the pressure and flow rate of fluid under complex conditions, we can

use the Navier–Stokes equations, which describe the motion of viscous fluids. The Navier–Stokes equations mathematically express the conservation of momentum and conservation of mass for Newtonian fluids (Constantin and Foias 1988). Although this equation is useful because it can describe many phenomena in fluidic engineering, it has not yet been proven to have smooth solutions. The equation can be written as

$$\frac{D\mu}{Dt} = \frac{1}{\rho}\nabla \cdot \sigma + f \tag{10.16}$$

where μ, t, ρ, σ, and f are the flow velocity, time, density, stress tensor, and body forces, respectively; $D\mu/Dt$ and $\nabla \cdot \sigma$ are the material derivative of μ and the divergence of the stress tensor, respectively.

2. **Design and Modeling**

Soft fluidic actuators have been designed using conventional three-dimensional (3D) computer-aided design (CAD) software. Because fluidic actuators relate to two or more fluid-related fields, including mechanics (large deformation), electronics, and chemistry, the design and modeling methods can be categorized into three types: empirical methods, mathematical methods, and finite element methods (FEMs). As fast design methods, empirical methods are primarily based on experimental results. Mathematical methods are beneficial for designing simple fluidic actuators with eccentric or three chambers, which can be easily explained on the basis of the Euler–Bernoulli beam theory. Even fluidic actuators subjected to external loads have been modeled in terms of edge and tip loading via a mathematical method. However, in some cases of delicate structures, explaining the relationship between the deformation and applied pressure through mathematic models is difficult. To address these limitations, more precise FEM models have been developed to optimize actuator geometry and couple it with large deformations of soft fluidic actuators.

10.2.3   Fabrication Techniques

Soft fluidic actuators can be fabricated using molding replication, 3D printing technology, or digital additive manufacturing. Among these, the most popular process is molding the elastomeric material to a structure with a fluid pathway and then adhering it to other fabricated molds (Shepherd et al. 2011). Fibers can be added to further modify the stiffness of soft actuators. The process mainly includes three steps: (a) preparing molds using machining or 3D printing technology; (b) casting the elastomer liquid into the molds; and (c) curing the elastomer using a thermal polymerization or photopolymerization process and subsequently removing the mold (Fig. 10.9a). Fluidic actuators can be fabricated at the microscale using stereolithography techniques. These miniature soft fluidic actuators can potentially be used in medicine (e.g., microsurgery). In addition, 3D printing technology (e.g., digital mask projection stereolithography) (Peele et al. 2015) and direct ink writing (Robinson et al.
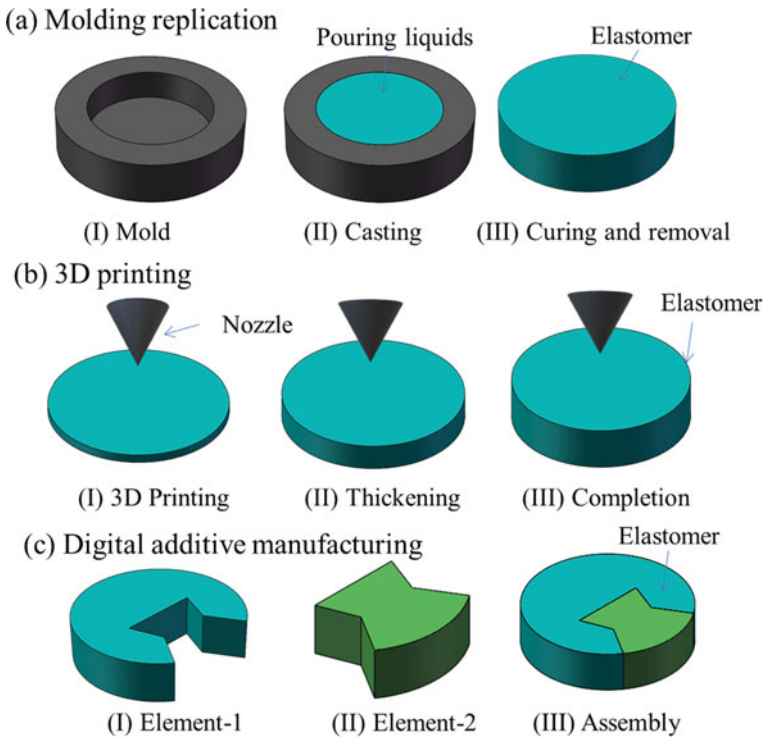
Fig. 10.9 Fabrication techniques: **a** molding replication, **b** 3D printing technology, and **c** digital additive manufacturing

2015) have been explored as alternative methods of producing soft fluidic actuators directly (Fig. 10.9b). Moreover, the digital additive manufacturing method is now emerging as a method for manufacturing soft actuators (Fig. 10.9c). The digital manufacturing method takes advantage of simple assemblers to complete traditional and complicated manufacturing tasks, similar to the use of tiles and bricks (Morin et al. 2014). The motions of soft fluidic actuators can be programmed by changing the stiffness of each block in the body. In addition, multifunctional devices can be realized by modifying internal structures.

10.2.4　Fluidic Pressure Sources

Fluid soft actuators are stretchable. However, their power source is often bulky and not entirely soft. Although numerous methods of driving fluidic actuators have been developed, we here focus on the actuators that operate on the basis of internal pressurization induced by fluids. The choice of fluid depends largely on the application. Fluids help produce large forces at the expense of increased viscosity and

weight. Here, we do not consider micropumps because it is difficult to power soft robots through them. The pressure sources of soft actuators can be mainly categorized into two types: offboard and onboard pumps. An offboard pump can be (a) an air compressor/microcompressor (Onal et al. 2017) (Fig. 10.10a), (b) mechanical hydraulic pump (Fig. 10.10b) (Katzschmann et al. 2018; Aubin et al. 2019; Xu et al. 2017), (c) thermomechanical pump (Garrad et al. 2019; Tse et al. 2020) (Fig. 10.10c), or (d) an electrostatic pump (Fig. 10.10d) (Acome et al. 2018; Diteesawat et al. 2021). An onboard pump can be (e) a chemical reaction pump (Fig. 10.10e) (Tolley et al. 2014; Wehner et al. 2016; Suzumori et al. 2013) or (f) a direct electricity–fluid conversion pump (Fig. 10.10f) (Cacucciolo et al. 2019; Mao et al. 2021).

1. **Air Compressor/Microcompressor (McKibben Artificial Muscle)**

Air pressure in soft robots is extensively used in many surgical robots, therapeutic applications, and wearable devices. Air, compressed by mechanical pumps, can be stored and released via various methods. Energy is transferred to the actuators as the pressurized air expands. Many soft actuators have been powered by an offboard air compressor or microscale air compressor to achieve simple or sophisticated motions. As one of the most efficient and commonly used fluidic artificial muscles, the McKibben artificial muscle is a prominent invention because of its simple design and the similarity of its behavior to that of human muscles (Kurumaya et al. 2016). The McKibben artificial muscle has an inner elastic tube, which is surrounded by
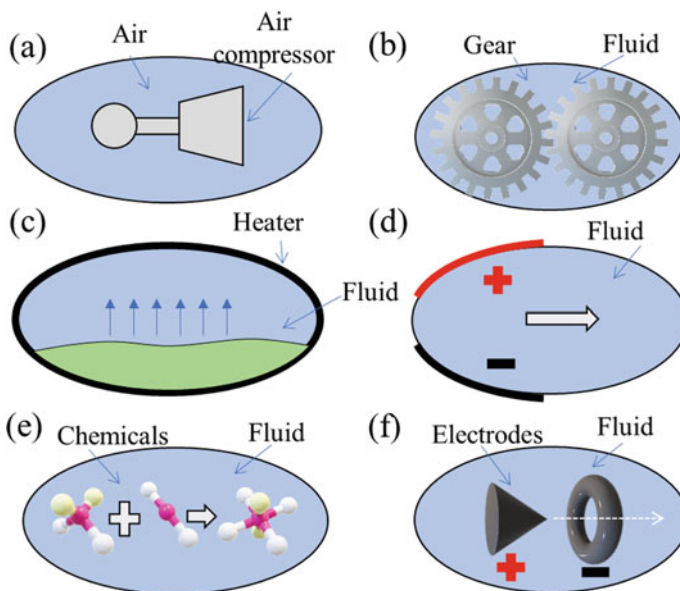

Fig. 10.10 Fluidic pressure sources: **a** air compressor/microcompressor, **b** mechanical hydraulic pump, **c** thermomechanical pump, **d** electrostatic pump, **e** chemical reaction pump, and **f** direct electricity–fluid conversion pump

Fig. 10.11 Simplified
geometrical model of a
McKibben artificial muscle,
where L is the initial length,
L_0 is the length after
stretching, α_0 is the initial
braid angle, F is the
actuating force, and D_0 is the
initial muscle diameter
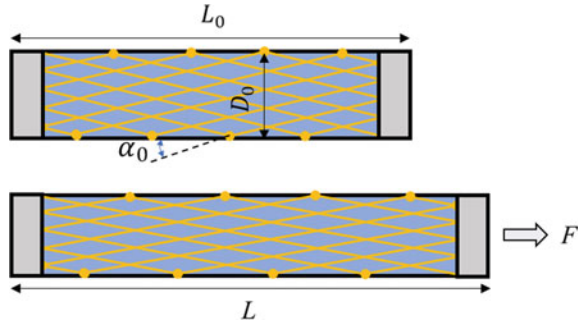
a double-helix-braided sheath (Fig. 10.11). The artificial muscle contracts when an
internal pressure exists and returns to its original shape as the pressure is released.
Therefore, if the McKibben artificial muscle is assumed to be completely cylindrical
and distortion effects from the two ends and the frictional force between the flexible
tube and mesh are neglected, the internal pressure (P) is given by

$$P = \frac{4F \sin^2 \alpha_0}{\pi D_0^2 \{3(1 - \varepsilon)^2 \cos^2 \alpha_0 - 1\}} \tag{10.17}$$

where F, α_0, ε, and D_0 are the actuating force, initial braid angle, contraction rate,
and the initial muscle diameter, respectively. The contraction rate can be defined as

$$\varepsilon = \frac{L - L_0}{L_0} \tag{10.18}$$

where L and L_0 are the initial nominal length and the length after stretching,
respectively.

2. **Mechanical Hydraulic Pump (Gear Pump)**

Pneumatic energy sources are extensively used for actuating soft robots on the
ground. By comparison, fluidic actuating systems can be used in underwater envi-
ronments. Offboard fluidic pumps, which include gear pumps and impeller pumps,
are often rigid mechanical moving parts integrated with several rigid components
such as rotating valves. Such offboard pumps are also used in several systems such
as sophisticated soft robotic fish (Katzschmann et al. 2018), electrolytic vascular
systems (Aubin et al. 2019), and traditional fluidic systems (Xu et al. 2017). Because
gear pumps have been reported to drive soft fluidic actuators, we here focus on gear
pumps in terms of their working principle (Katzschmann et al. 2018).

The operating principle of gear pumps is to use the meshing of gears to pump
fluids via displacement. As the gears rotate in the pumps, the void between two
gears is occupied by the fluid. The gears then carry the fluid from the inlet to the
outlet of the pump. Because of tight mechanical tolerances, leakage of liquid to the
inlet can be effectively prevented. This meticulous design enables the pumping of

high-viscosity fluids. Structurally, gear pumps are divided into two main groups: internal and external gear pumps. The external gear pumps have two external spur gears, whereas the internal ones have an internal and external spur gear. A gear pump can produce a fixed-volume displacement; thus, the volumetric displacement can be described using

$$V = \frac{\pi}{4}\left(D_{\mathrm{o}}^2 - D_{\mathrm{i}}^2\right)L \tag{10.19}$$

where D_{o}, D_{i}, and L are the outer diameter, inner diameter, and width of the gear teeth, respectively.

3. **Thermomechanical Pump (Ball Actuators)**

A thermomechanical pump relies on the use of low-boiling point fluids (LBPFs), which can be transformed from the liquid state to the gaseous state by controlling the temperature (Garrad et al. 2019). In principle, exterior heat causes LBPFs to boil in the closed chamber, thus causing a shape change. This pump is highly compatible with FEAs because the fluids used in FEAs can be selected on the basis of their ability to undergo the liquid–gas phase change. When a compliant heating element is used, the phase-change process can function as a power source to actuate the gas. Also, other pumps based on the thermomechanical mechanism have been developed using super-coiled polymer (SCP) artificial muscles (Tse et al. 2020). The pump's structure is composed of a flexible bellow and SCP artificial muscles. Models of these two thermomechanical pumps are still under development.

4. **Electrostatic Pumps (Hydraulically Amplified Self-healing Electrostatic [HASEL] Actuators)**

Electrostatic actuators are attractive because they operate silently and exhibit high energy efficiency and self-sensing properties. By exploiting the electrical and hydraulic properties of dielectric fluids, researchers have developed some interesting actuators, including hydraulically amplified self-healing electrostatic (HASEL) (Acome et al. 2018) and electro-ribbon actuators. Structurally, two electrodes are zipped to pump the liquid via electrostatic forces. To complete the zipping process, a small amount of dielectric liquid is required to ensure that the two electrodes are placed at the closest possible position. When dielectrophoretic liquid zipping (DLZ) is used, this pump can pump either a gas or a liquid. The output energy ($E_{\mathrm{output}}(t)$) can be described using (Diteesawat et al. 2021)

$$E_{\mathrm{output}}(t) = (P_{\mathrm{atm}})(V_{\mathrm{in}} + V_{\mathrm{connector}}) \cdot \log\left(\frac{P_{\mathrm{i}} + P_{\mathrm{atm}}}{P_{\mathrm{a}}(t) + P_{\mathrm{atm}}}\right) \tag{10.20}$$

where P_{atm}, V_{in}, $V_{\mathrm{connector}}$, P_{i}, and $P_{\mathrm{a}}(t)$ are the atmospheric pressure, injected air volume, volume of the connecting tube, input power, initial pressure at no actuation, and the actuated pressure at time t, respectively.

5. **Chemical Reaction Pump (Combustion Actuators)**

Chemical reactors, such as those that operate by combustion (methane (butane) + oxygen) or peroxide decomposition, have been developed to realize directional jumping maneuvers and soft, autonomous robots (Tolley et al. 2014; Wehner et al. 2016). This type of pressure source can be operated portably and can generate pressurized gas or new chemicals using combustible fuels. To maximize the energy density of the fuel, pure oxygen is used instead of air. In this pump, an enriched oxygen environment is provided by the catalytic decomposition of H_2O_2. In the presence of a Pt catalyst, the following reaction occurs:
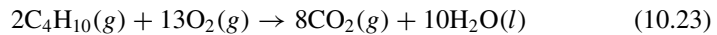
$$2H_2O_2(l) \rightarrow 2H_2O(l) + O_2(g) \tag{10.21}$$
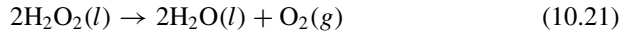
Methane and butane are used as fuel because they are easily controlled to ignite the reaction, are commercially available, release sufficient energy, and work over a wide temperature range (Tolley et al. 2014; Wehner et al. 2016).

For methane, the reaction follows:

$$CH_4(g) + 2O_2(g) \rightarrow CO_2(g) + 2H_2O(l) \tag{10.22}$$
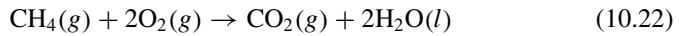
For butane, the reaction follows:

$$2C_4H_{10}(g) + 13O_2(g) \rightarrow 8CO_2(g) + 10H_2O(l) \tag{10.23}$$

If the temperature at the moment of ignition and the temperature after the combustion reaction are represented as T_1 and T_2, respectively, the generated pressure of the pump can be calculated as

$$P_2 = P_1 \frac{T_2}{T_1} \tag{10.24}$$

where P_1 and P_2 are the pressure at the moment of ignition and after the combustion reaction, respectively.

To achieve not only gas generation but also gas absorption, the following reversible chemical reaction can be used for driving fluidic actuators:

$$2H_2O(l) \rightarrow 2H_2(g) + O_2(g) \tag{10.25}$$

$$2H_2(g) + O_2(g) \rightarrow 2H_2O(l) \tag{10.26}$$
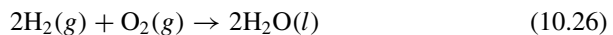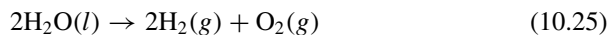
6. Direct Electricity–Fluid Conversion Pump (Electrohydrodynamic Pump)

Fluidic pressure can be achieved using functional/dielectric liquids under applied high voltages. The viscous forces generated by the liquid are used to drive the actuator. This pump, known as an electrohydrodynamic (EHD) pump, has been widely researched in recent years (Cacucciolo et al. 2019; Mao et al. 2021). The EHD jet can

be observed when the electrodes are connected to a power source. The EHD effect is governed by the electric force ($\vec{F}$), which can be expressed as (Stratton 2007)

$$\vec{F} = q\vec{E} - \frac{\varepsilon_0}{2}E^2\nabla\varepsilon_{\mathrm{r}} + \frac{\varepsilon_0}{2}\nabla\left(E^2\frac{\partial\varepsilon_{\mathrm{r}}}{\partial\rho}\rho\right) \qquad (10.27)$$

where q, ρ, $\vec{E}$, ε_0, and ε_{r} are the charge density, density of the dielectric liquid, electric field, permittivity of vacuum, and the relative permittivity of the dielectric liquid, respectively. The electric forces include three types of forces—Coulomb force, dielectric force, and electrostriction force—that contribute to the pressure and flow rate of EHD pumps. In addition, the EHD flow can be described using the Navier–Stokes equation as follows:

$$\frac{\partial\vec{\mu}}{\partial t} = -(\vec{\mu}\cdot\nabla)\vec{\mu} - \frac{1}{\rho}\nabla p + \frac{\eta}{\rho}\nabla^2\vec{\mu} + \frac{1}{\rho}q\vec{E} \qquad (10.28)$$

where $\vec{\mu}$, p, and η are the velocity, pressure, and viscosity, respectively. EHD jets and pumps have been used to drive various interesting actuators (e.g., finger, hand, and soft fish actuators).

10.2.5   Challenges

1. *Soft powerful and continuous pressure sources onboard*

Currently, most robotic systems in laboratories are strongly dependent on rigid, heavy, offboard power sources (e.g., air compressors or hydraulic pumps). These offboard pumps cannot easily be softened. Onboard pumps, such as chemical pumps that use combustible fuels, can generate instantaneous pressure. The reliability of the interfaces between the integrated electrical, chemical, pneumatic, and hyperplastic systems is still under investigation because the explosive forces can easily disable the system. Also, refilling fuel for chemical pumps is cumbersome and requires disassembling the robot, which eventually leads to difficulty in generating continuous pressure. In addition, direct electricity–fluid conversion pumps usually generate limited pressure, which makes actuating soft systems with loads difficult. Therefore, the development of soft, powerful, and continuous onboard pressure sources is urgently needed for fluidic actuators.

2. *Modeling of fluidic actuators driven by pressure sources*

Fluidic actuators powered by offboard pumps have been extensively studied because hydraulic and pneumatic systems have been well developed. In addition, two models for the relationship between hyperplastic deformation and fluidic systems have been developed. However, fluidic actuators driven by onboard pumps are difficult to model because their technology spans several fields, including the fluid, hyperplastics,

chemical, and electrical fields. This complexity complicates the modeling process for fluidic actuators, making dynamic models, in particular, difficult to develop.

3. *Untethered soft fluidic systems on the ground*

An autonomous, mobile system is necessary as an imperative part of the field of human–robot interactions, such as in search and rescue operations. However, most robotic systems in laboratories are strongly dependent on rigid and heavy power sources (air compressors or hydraulic pumps) connected via electrical tethers. Carrying heavy power sources and overcoming gravity can disable the locomotion of soft robots. Although untethered mobile systems that operate underwater have been developed, an untethered system (Kitamori et al. 2016) on the ground remains a formidable challenge in this field because the robots' ability to lift against gravity and the supply of power must be considered.

10.3 Electroactive Polymer Actuators

Electroactive polymers (or electromechanically active polymers, EAPs), refer to polymers that deform in response to external electric stimuli (Bar-Cohen 2004; Carpi 2016). EAPs are often referred to as artificial muscles because of the ability of the material to deform in response to stimuli (Mirvakili and Hunter 2018). In addition, these polymers are smart materials as they can be used to perform sensing and actuation (Shahinpoor 2020).

Two types of EAPs are widely used in soft robotics: dielectric elastomer actuators (DEAs) and ionic polymer–metal composites (IPMCs) (Carpi 2016; Shahinpoor 2020). Both materials deform in response to electrical stimuli. The difference is that in the case of the former material, the attraction of opposing electric charges directly moves the structure, whereas in the case of the latter material, the actuation is performed by the physical movement of mobile cations, that is, positively charged ions.

In the recent decade, DEAs and IMPCs have contributed to advancements in the field of soft robotics. This section describes the underlying principles, characteristics, materials, manufacturing methods, and applications of the two types of EAP actuators.

10.3.1 DEAs

Positive and negative charges attract each other. This attractive force, that is, the Coulomb force or electrostatic force, is the driving force for DEAs. Although the electrical deformation of solid materials was observed in the late eighteenth century, the operating principles of DEA were established in the late 1990s (Pelrine et al. 1998).
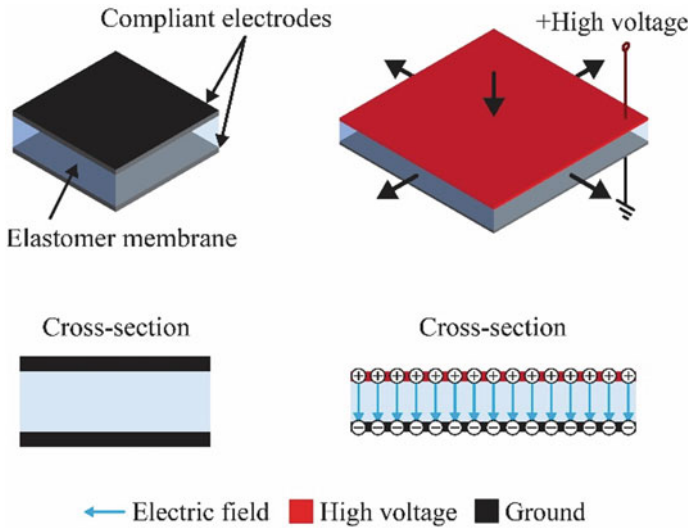
Fig. 10.12 Working principle of dielectric elastomer actuators (DEAs)

A typical DEA consists of a thin elastomer membrane sandwiched between compliant electrodes, as shown in Fig. 10.12. Elastomer is a general term for polymers with viscoelasticity. The Young's modulus of elastomers used in DEAs ranges from 0.1 to 1 MPa. When a high potential difference of several kV is applied between the electrodes, the elastomer membrane compresses in the thickness direction and expands in the planar direction as the opposing charges on the electrodes experience attraction. This deformation can be exploited as actuation motion. In addition, the current flowing through DEAs during actuation is approximately 100 μA because of the electrostatic nature.

DEAs can generate large deformations of over 100% strain with a fast response time of a few milliseconds and a high energy density of more than 3 MJ/m^3. Moreover, because of their simple structure, the electromechanical efficiency of DEAs, which is the rate of conversation of electrical input into mechanical output, is theoretically more than 90%.

The fundamental characteristic of DEAs, which enables the interconversion of electrical and mechanical inputs and outputs, is quasi-reversibility. Owing to this property, DEAs are often termed dielectric elastomer transducers. This property allows DEAs to be used as sensors or energy harvesting elements. DEAs, which have a simple structure consisting of an elastomeric membrane and a couple of electrode layers, can be used in a diverse range of actuator configurations. Moreover, these actuators can be adopted in robots of various forms in a wide range of scales, from millimeters to meters. In addition, DEAs, as mechatronic elements, have been applied in various scientific fields. Details regarding these applications can be found in the literature (Brochu and Pei 2010; Anderson et al. 2012; Rosse and Shea 2016; Gu et al. 2017; Guo et al. 2021).

Working Principle

In the actuation of DEAs, the electrostatic force that compresses the elastomer membrane in the thickness direction is known as the Maxwell stress and can be expressed as

$$\sigma_{\mathrm{M}} = \varepsilon_0\varepsilon_{\mathrm{r}}E^2 = \varepsilon_0\varepsilon_{\mathrm{r}}\left(\frac{V}{d}\right)^2 \tag{10.29}$$

where ε_0 and ε_{r} denote the permittivity of free space and relative permittivity (or dielectric constant) of the elastomer, respectively. E is the electric field between the electrodes, which is a product of the voltage potential difference V and membrane thickness d. Using Eq. (10.29), the strain in the thickness direction can be defined as

$$S_z = -\frac{\sigma_{\mathrm{M}}}{Y} = -\frac{\varepsilon_0\varepsilon_{\mathrm{r}}E^2}{Y} \tag{10.30}$$

where Y is the Young's modulus of the elastomer. The sign of the strain is negative because the deformation is induced in the direction of decreasing membrane thickness. Assuming that the elastomer membrane is incompressible, that is, its volume is constant under deformation and the Poisson's ratio approaches 0.5 (as in the case of most elastomeric materials), the strains in the planar directions can be defined as

$$\begin{aligned}(S_x + 1)(S_y + 1)(S_z + 1) &= 1\\ \therefore S_x = S_y &= (S_z + 1)^{-\frac{1}{2}} - 1\end{aligned} \tag{10.31}$$

Equations (10.29) and (10.30) indicate that the actuation of DEAs is proportional to the relative permittivity, square of the electric field, and inverse of the Young's modulus. These equations can guide the selection and study of materials for DEAs. In general, soft elastomers that exhibit a high relative permittivity and dielectric strength are promising candidate materials. To enhance the relative permittivity and dielectric strength, fillers can be added to the elastomer materials, or the elastomeric membrane can be prestretched. The degree of prestretching determines the behavior of actuation. It has been experimentally demonstrated that prestretching an elastomer enhances its dielectric strength (Huang et al. 2012). Moreover, Eq. (10.29) indicates that a target actuation output can be achieved at low voltages with small membrane thicknesses. Therefore, previously, we focused on developing thin DEAs driven at certain voltages (for instance, to realize actuation below 500 V (Ji et al. 2018)).

Equations (10.29)–(10.31) represent the simplest and most basic expressions for modeling the actuation behavior of DEAs. However, the results often lack accuracy, particularly in the case of large deformations. In such cases, a hyperelastic material model that can consider the high stretchability and nonlinearity of elastomers can be used in analytical analyses, or a finite element analysis software can be used to model the actuator. ABAQUS (Dassault Systemes Co. Ltd.) and ANSYS (Ansys Software Pvt. Ltd.) are typical finite element analysis software used for such modeling. When

modeling DEAs, the presence of electrodes must be considered to obtain accurate predictions. In particular, electrodes are passive elements, and their stiffness and dimensions can affect the amount of resulting actuation.

Materials and Fabrication Methods

Acrylic and silicone materials are mainly used to prepare elastomeric membranes in DEAs. Acrylic elastomers usually correspond to a high output but low response speed, and silicone elastomers correspond to a low output but high response speed. Several types of these materials are commercially available as cured and formed tapes or sheets, for instance, as VHB 4905/4910 (3M Co. Ltd.) and ELASTOSIL Film 2030 (Wacker Chemie AG), which represent acrylic and silicone elastomers, respectively.

Despite the easy availability of such materials, commercial elastomers are often provided in an uncured, liquid state. Consequently, membrane fabrication must be performed, such as forming the material into a thin layer and curing it, and the related equipment must be procured. Thin elastomeric membranes can be prepared through centrifugal spin coating, spray coating, inkjet printing, 3D printing, pad printing, or blade casting. The formed membranes are then cured by heat or light, depending on the material characteristics.

Electrodes in DEAs can be prepared using a wide variety of materials, such as carbon grease, carbon black, carbon nanotubes, graphene, metal particles, silver nanowires, liquid metals, and conductive gels. These materials can be mixed with elastomers to endow conductivity. These electrode materials can be applied to the elastomer manually using a brush or in a manner similar to the thin-film forming process described previously.

Actuator Configurations

The actuator configuration is of significance to decrease the thickness and increase the area of the elastomeric film for usable movement.

Figure 10.13a summarizes the representative configurations of DEA prepared in the early stages of development (late 1990s to early 2000s), specifically, diamond-shaped, rolled, tubular, planer, folded, and bended configurations. In the diamond-shaped form, the expansion of DEA is converted into vertical extension using a structure equipped with flexible hinges. When a DEA is rolled, it exhibits elongation in the longitudinal direction. The tubular form operates with a similar principle, but its internal structure is hollow. In the planar form, the expansion of the DEA area is exploited as deformation in the plane. The movement direction depends on the shape of the DEA. For example, in the rectangular form, the lengthwise elongation is dominant. The elongation is transformed to bending actuation when a DEA is laminated onto a hinged structure or a flexible substrate, as in the folded and bended forms. The use of a hinged structure or flexible frame enables folding of the entire structure owing to the mechanical compliance. Notably, these configurations rely on the area expansion of the DEA. If thickness reduction is employed as the main actuation principle, the actuator exhibits a linear contraction such as that in a muscle.

This type of configuration is prepared by stacking multiple DEAs or folding a long DEA, as shown in Fig. 10.13b.

Soft Robotic Applications

The intrinsic compliance and diverse actuator configurations of DEA have enabled the development of various soft robots. Figure 10.14 shows several representative soft robotic applications based on DEAs. A soft gripper, shown in Fig. 10.14a, is suitable for grasping several types of objects. The device compliance allows the gripper to conform to the target in contact (Shintake et al. 2016, 2018a). This structural conformation at the interface is a type of automated behavior that simplifies control, and in certain cases, enables the accomplishment of tasks with only an on/off input.

As mentioned, DEAs operate through the application of a high potential difference of several kV. This aspect appears to imply that a high-voltage power supply or converter must be used to drive the actuators. However, miniaturized DC/DC converters, weighing only a few grams, can be used. Using such devices, untethered
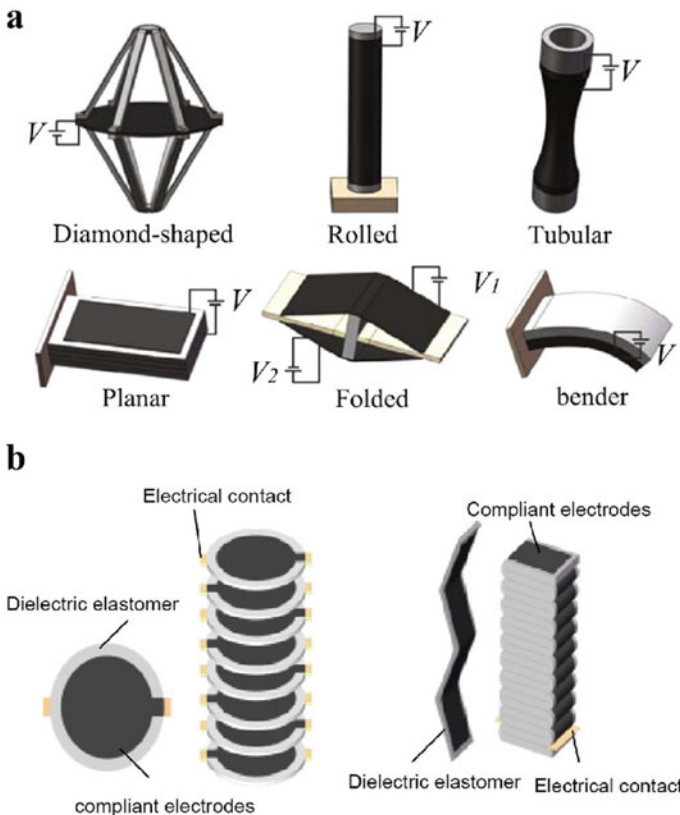

Fig. 10.13 **a** Typical configurations of DEAs, adopted from Gu et al. (2017). **b** Stacked and folded configurations, adopted from Wang et al. (2018)
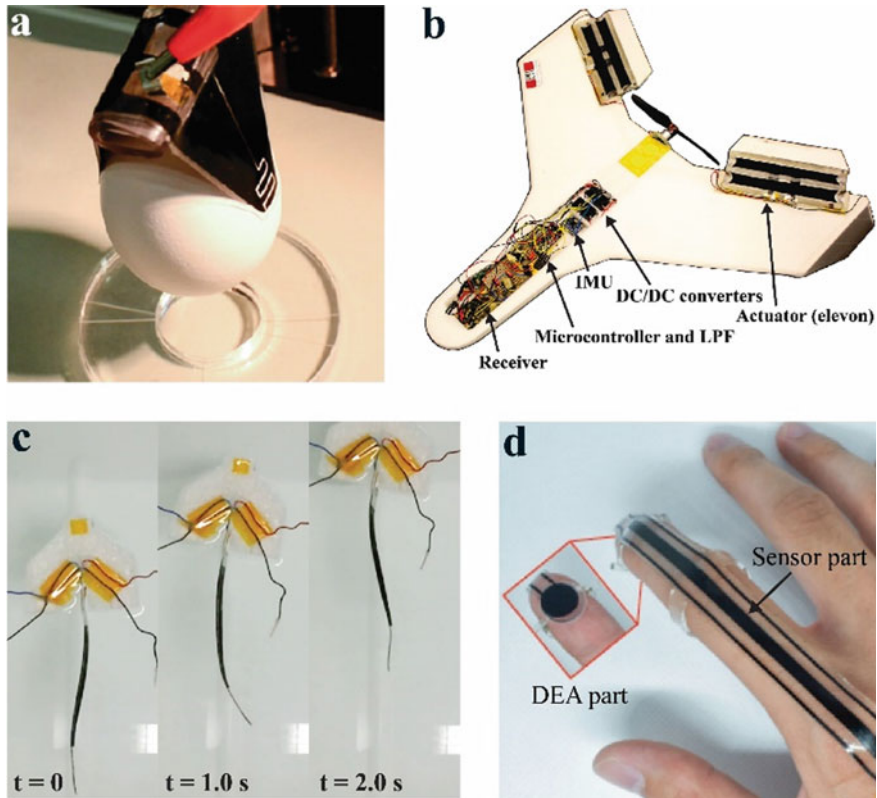
Fig. 10.14 Representative soft robotic applications based on DEAs. **a** Soft gripper. **b** Flying drone. **c** Underwater robot. **d** Multifunctional wearable device

DEA robots containing all the components, such as a driving circuit, controller, and battery, can be prepared. A representative device is shown in Fig. 10.14b, that is, a small flying drone with control surfaces made of DEAs (Shintake et al. 2015).

With sufficient insulation, DEAs can operate underwater. This property can enable the development of biomimetic underwater robots, as shown in Fig. 10.14c (Shintake et al. 2018b). In such robots, the short-circuiting of electrodes on the high-voltage side is prevented, although the electrodes on the outside are often not insulated. This configuration is established because the water surrounding the robot is used as the electrode on the ground side.

Because DEAs are soft and thin, they can conform to the surface of the human body and thus promote the realization of wearable systems. An example is haptic devices that can apply vibration and force. As shown in Fig. 10.14d, a circular DEA attached to the thumb can provide a vibrating haptic sensation, and through its multifunctional nature, it can detect bending deformation of the finger (Kanno et al. 2021).

This discussion demonstrates the high applicability of DEA to soft robotics. More types of robots, including practical systems, can be expected to be realized in the future.

10.3.2 IPMCs

IPMCs consist of a cation exchange resin membrane (thickness: 100–300 μm) with flexible electrodes attached on both sides (Asaka et al. 1995). To prepare the membrane, a sulfonated tetrafluoroethylene-based fluoropolymer-copolymer, also known as Nafion (DuPont Inc.), is commonly used because of its high water content ratio and cation exchange capacity. Gold and platinum are commonly used to prepare electrodes, although carbon materials, particularly carbon nanotubes, have attracted attention recently. Moreover, IPMCs can function as sensors or as polymer electrolyte fuel cell membranes for pumping fluid-driven soft actuators (Nabae et al. 2019).

A typical structure of IPMCs is illustrated in Fig. 10.15a. When a potential difference of a few volts (1–3 V) is applied to the electrodes, the cations in the membrane migrate to the negative side. This movement causes the negative side of the membrane to swell and the entire structure to bend toward the positive side, leading to a bending motion defined as actuation. The deformation of IPMCs is large, and more than 180° of bending actuation can usually be achieved. Because the actuation principle relies on the physical movement of ions, the speed of actuation is relatively low. An energy density of 5.5 kJ/m^3 has been reported (Park et al. 2008).

When an IPMC is bent by an external force, it generates a voltage of 0.1–1 mV corresponding to the amount of deformation, which allows it to act as a sensor, as represented in Fig. 10.15b. When water is filled around an IPMC and voltage is applied to the electrodes, hydrogen and oxygen gases are generated by electrolysis, as displayed in Fig. 10.15c. When the voltage application is terminated, water is synthesized by the gases. In this manner, the IPMC functions as a chemical pump for fluid-driven soft actuators.

As mentioned, gold is usually used to prepare the electrodes in IPMC actuators, although several researchers have employed platinum as well. Notably, platinum is extremely hard to bend and is often damaged by actuator movements. Gold is relatively soft and does not incur damage during actuation. To attach gold electrodes to a cation exchange resin membrane, non-electrolytic plating must be performed to ensure the mobility of ions between the membrane and electrodes, which is essential for actuation.

For IPMC sensors, non-electrolytic plating does not need to be performed. Instead, metal sheets can be simply placed on the surfaces of the cation exchanger resin membrane. However, the caustic action of the membrane must be addressed. For example, Nafion includes a sulfonate group, which acts as an acid and base in the presence of H$^+$ and Na$^+$, respectively. Therefore, aluminum and copper cannot be used as the electrodes because they will melt. In such scenarios, corrosion-resistant metals such as stainless and gold can be applied.
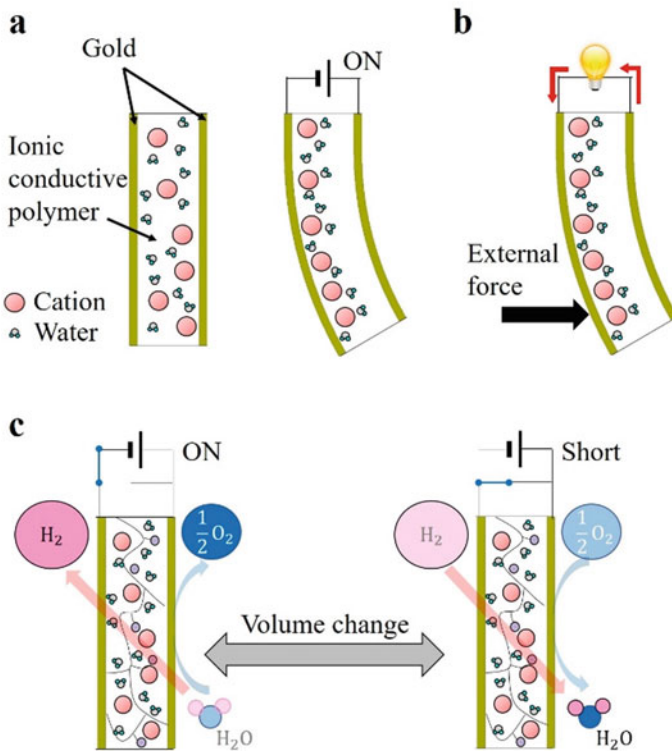
Fig. 10.15 Working principles of IPMCs. **a** Actuation. **b** Sensing. **c** Chemical pumping

Working Principle of IPMC Actuators

The performance of IPMC actuators is highly influenced by the length and thickness of the cation exchange resin membrane. Consequently, the geometric design of the actuator is of significance.

In a bending state, as shown in Fig. 10.16, the deformation of the actuator can be considered as strain in an infinitesimal interval of its length $\Delta l/l$, where l is the length of the device. The strain is influenced by the size and number of cations and magnitude of the applied voltage. In the case of thick IPMC actuators, the surface area and thickness of the electrodes are also important. In particular, to generate a large actuation, a material with large cations (for example, tetramethylammonium) must be used. Furthermore, increasing the membrane roughness by sandblasting prior to attaching the electrodes also increases the strain.

The strain of the actuator $\Delta l/l$ can be calculated considering the radius of curvature R. As shown in Fig. 10.16, Δx and L_{dis} are defined as the tip displacement and length between the actuator base and measurement point, respectively. Using the Pythagorean theorem, we obtain
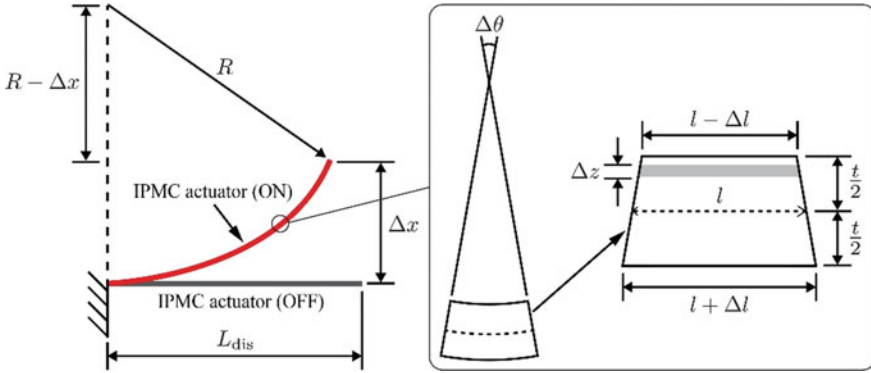
Fig. 10.16 Schematic of an IPMC actuator in a bending state

$$R^2 = (R - \Delta x)^2 + L_{dis}^2 \tag{10.32}$$

Transforming this equation yields the expression of R.

$$R = \frac{\Delta x^2 + L_{dis}^2}{2\Delta x} \tag{10.33}$$

The following relationship holds for R and the bending angle of infinitesimal interval, $\Delta\theta$.

$$\begin{cases} R\Delta\theta = l \\ \left(R + \frac{t}{2}\right)\Delta\theta = l + \Delta l \end{cases} \tag{10.34}$$

Transforming Eq. (10.34) yields

$$\Delta l = \frac{tl}{2R} \tag{10.35}$$

where t is the membrane thickness. The strain is defined as

$$\frac{\Delta l}{l} = \frac{t}{2R} \tag{10.36}$$

Substituting Eq. (10.33) into Eq. (10.36) yields

$$\frac{\Delta l}{l} = \frac{t\Delta x}{\Delta x^2 + L_{dis}^2} \tag{10.37}$$

According to Eq. (10.37), if $\Delta l/l$ is constant, t and Δx are nearly inversely proportional to each other. $\Delta l/l$ can be increased by increasing t because an actuator

with a large thickness has a large number of cations in the membrane. However, in this case, it is necessary to increase the surface area and thickness of electrodes.

The blocking force is another metric that represents the performance of IPMC actuators. The force can be calculated based on the power and moment generated by the expansion and contraction in an infinitesimal interval of an actuator. The moment M represents an integral ranging from $-t/2$ to $t/2$ of the moment of the volume illustrated in Fig. 10.16. M is calculated by multiplying the power by the distance from the neutral line in the actuator structure. The power is computed by multiplying the expansion by the spring rate, which is calculated using the Young's modulus of the cation exchange resin membrane E and actuator size.

$$
\begin{cases}
M = \int_{-t/2}^{t/2} \text{Power} \cdot z \mathrm{d}z \\
\text{Power} = \text{Expansion} \cdot \text{Spring rate} \\
\text{Spring rate} = E \frac{w \mathrm{d}z}{l} \\
\text{Expansion} = \Delta l \frac{z}{t/2}
\end{cases}
\tag{10.38}
$$

where w is the width of the actuator. Transforming Eq. (10.38) yields an expression of M as

$$
M = 2 \int_0^{t/2} \Delta l \frac{z}{t/2} E \frac{w}{l} \mathrm{d}z = E w t \frac{\Delta l}{l}
\tag{10.39}
$$

The blocking force F is defined as

$$
F = \frac{M}{L_{\text{force}}}
\tag{10.40}
$$

Equation (10.40) can be rewritten as

$$
F = \frac{E w t}{L_{\text{force}}} \frac{\Delta l}{l}
\tag{10.41}
$$

Equation (10.41) indicates that when the length of the actuator (L_{force}) is large, the blocking force decreases because of the principle of leverage. Moreover, increasing the width and thickness of the actuator increases the blocking force. As described previously, the strain $\Delta l / l$ can be increased by increasing the thickness. Therefore, increasing the thickness is the optimal approach to increase the power and thus the force.

Soft Robotic Applications

Owing to their low-voltage application and simple structure, IPMCs are widely applied in soft robotics. Figure 10.17 shows several representative soft robotic applications based on IPMCs. The early developments were focused on using IPMC actuators in a tethered condition, and promising applications such as soft grippers (Fig. 10.17a) and underwater robots (Fig. 10.17b) were demonstrated (Bar-Cohen et al. 1998; Takagi et al. 2006). Recently, untethered robots were developed, as shown in Fig. 10.17c, in which electrical components such as a controller and battery were included. Because IPMCs can be driven at low voltages, a single cell lithium polymer battery can adequately power all the electric components. The bending motion of the actuator can be transformed to inchworm-like locomotion that drives the robot forward.

In addition to soft robots, the low-voltage application of IPMCs renders them suitable for medical devices. A representative example is shown in Fig. 10.17d, indicating the use of IPMC actuators in intraocular lenses (Horiuchi et al. 2017).
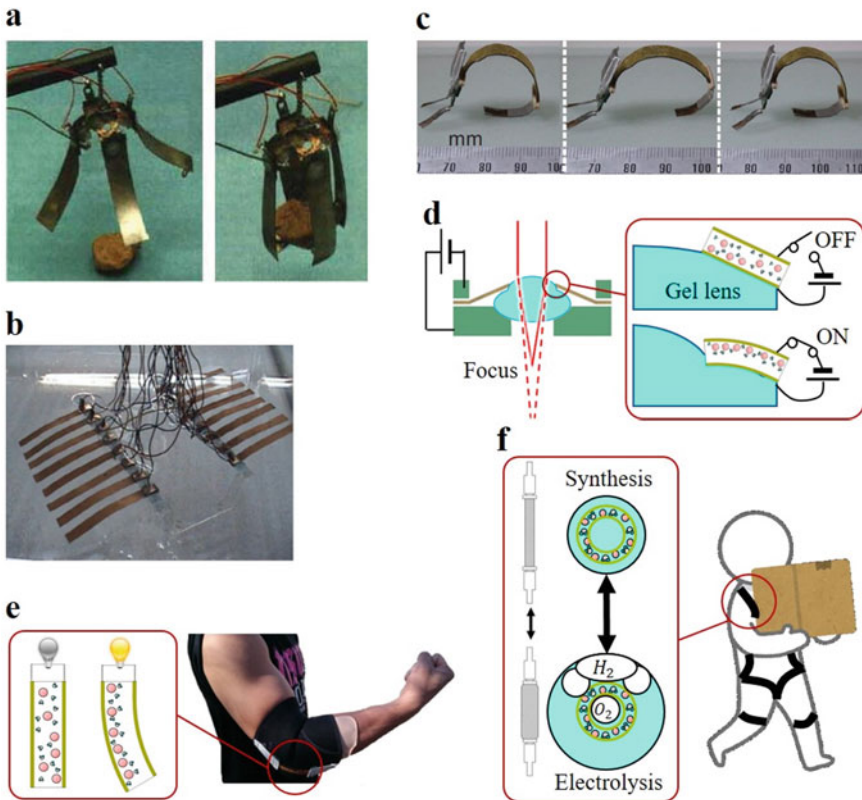

Fig. 10.17 Representative soft robotic applications based on IPMCs

Intraocular lenses are promising medical devices for cataract surgery. The extremely thin actuators can be used inside of the eye. When voltage is applied, the bending motion of the actuators deforms the gel lens part, leading to voltage-controlled focus change.

Another application of IPMCs is wearable devices to detect, for instance, the motion of a human joint, as shown in Fig. 10.17e. IPMC sensors are adequately soft to safely follow the deformations of the human body. When used as a chemical pump, IPMCs can drive power suits (Nabae et al. 2019), as illustrated in Fig. 10.17f. Conventional pneumatic power suits require the connection of tubes to supply air from an external source, which can limit the movement of workers wearing the device. IPMC pumps eliminate the need for introducing air tubes, and thus, the suits can be used in an untethered manner.

10.3.3 Future Outlook

Owing to their unique properties, such as intrinsic softness, simplicity, high performance, and multifunctionality, EAPs can serve as ideal actuators in soft robotics. To this end, further research and development must be performed in the areas of materials, structure, manufacturing, and implementation. These research efforts involve many scientific fields, such as materials, mechanics, electronics, and control. The advancement of EAP technology is expected to facilitate the development of soft robotics and related fields and to enrich future society.

10.4 Thermomechanical Actuators

10.4.1 Shape-Memory Alloy Actuators

A shape-memory alloy (SMA) is an alloy that remembers its original shape. It is deformable by the application of external force in the martensite phase at lower temperatures and returns to its pre-deformed shape when heated to transit into the austenite phase (Melton and Mercier 1981; Piao et al. 1992). Shape-memory alloys have been widely applied to various engineering and medical fields to introduce thermomechanical actuators such as shape-memory springs, thermo-reactive valves and catheters, and efficient energy transducers (Reynaerts et al. 1999; Singh et al. 2003; Kennedy et al. 2004; Fukui et al. 2004; Kim et al. 2006; Mizukami and Sawada 2006; Pan and Cho 2007; Juan et al. 2008; Bellini et al. 2009; Sun et al. 2011). Owing to their lightweight, compact size, and the generatable force, the SMA actuators are expected to act as alternatives to conventional electronic actuators, electric motors, and pneumatic and hydraulic actuators. Their transformation speed is, however, comparatively slow, since the phase transformation between the martensite and austenite phases is

led by the temperature, which is conducted by supplying heat to the material body or radiating heat to the surrounding environment.

A filiform SMA wire with the diameter of 50–100 μm presents unique characteristics, swiftly responding to temperature related to the martensite and austenite phases. By applying weak current to an SMA wire, heat is generated owing to internal resistance, and the wire shrinks by up to 5% lengthwise. When the current stops flowing and the temperature drops, then it returns to the original length. The SMA wire is thin and flexible enough to be cooled down right after the current stops flowing, and it returns to the pre-deformed length according to the temperature shifts from the austenite to martensite states. This means that the contraction and returning of the SMA wire can be precisely controlled by the properly prepared pulse current.

The authors have also discovered that the deformation caused by a given stress to a SMA wire generates a change in the electric resistance. With this characteristic, the SMA wire works as a force sensor with high sensitivity, while generating microvibration. The SMA wires have been applied to tactile displays and sensors that react to the force applied to the display by a user as a feedback (Hafiz and Sawada 2011; Zhao et al. 2012; Takeda and Sawada 2013; Jiang et al. 2014; Danjo et al. 2016, 2017; Geier et al. 2020; Chen et al. 2020). The detailed properties of an SMA wire are introduced herein, together with possible robotic applications.

10.4.2   Physical Properties of SMAs

SMAs display two representative effects as physical properties related with the body temperature and the applied force; they are the shape memory effect and pseudoelasticity, as shown in Fig. 10.18.

The shape memory effect, shown in blue in Fig. 10.18, is observed as a result of heat exchange in the body. An SMA in the martensite state is deformable under the application of a load, and the shape returns to the original one by receiving heat to transit to the austenite state. The transition between the martensite and austenite states is reversible under the application of heat to the body or the radiation of heat from the body.

The pseudoelasticity, on the other hand, is the phenomenon observed in the austenite phase, shown in orange in Fig. 10.18. A loaded SMA in the austenite state shows the deformation to transit to the martensite state, which is called stress-induced martensite phase, and the strain is released by removing the load. This transformation exhibits the change of electric resistance, and in particular, the transformation between the austenite state and R-phase shows a quick response in time.
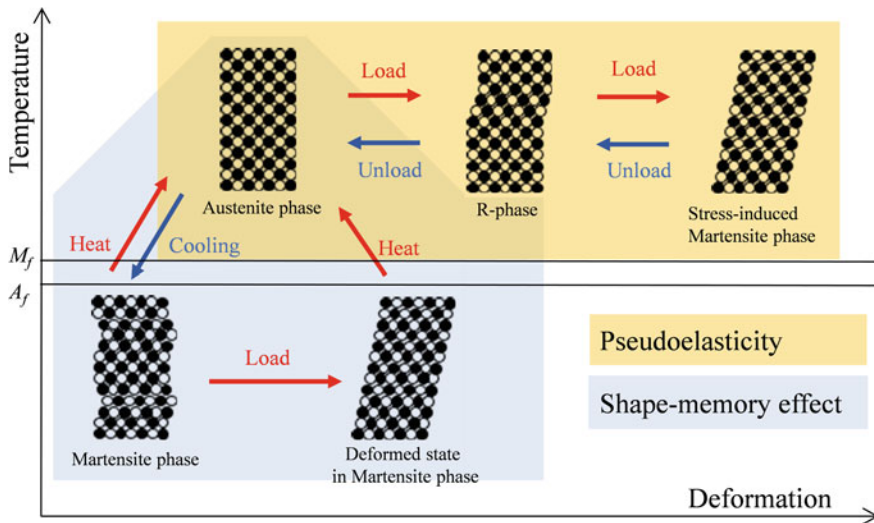
Fig. 10.18 Physical properties of the deformation of a SMA

10.4.3   Filiform SMAs for Micro-vibration Actuators

The authors have developed a micro-vibration actuator electrically driven by pulsed current. Figure 10.19 shows a vibration actuator composed of a 5-mm-long SMA wire with a diameter of 0.05 mm. On applying weak current to the alloy, the temperature rises to T_2 owing to the heat generated inside the wire body, and the length of the alloy shrinks by up to 5% of the original length. When the current stops flowing and the temperature drops to T_1 owing to heat radiation, the alloy returns to its original length. Figure 10.20 shows the temperature characteristics of the SMA wire employed in this study having the specific temperatures $T_1 = 68°$ and $T_2 = 72°$ (Mizukami and Sawada 2006).

The SMA wire is so thin that it rapidly cools down after the current stops flowing and returns to its original length when the temperature shifts from T_2 to T_1. This
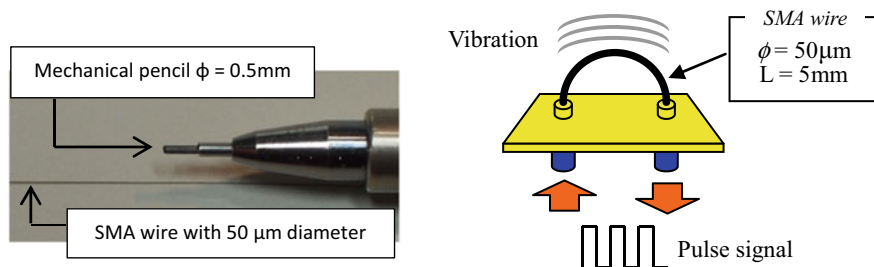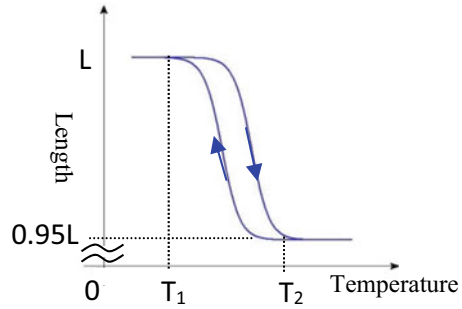

Fig. 10.19   SMA wire and vibration actuator

Fig. 10.20 Temperature characteristics of an SMA wire

means that the shrinkage and the return to initial length of the SMA wire can be controlled by controlling the pulse current. By driving the SMA wire with pulse current as shown in Fig. 10.21, micro-vibration with an amplitude of several micrometers is generated, which is perceived by the human body as tactile sensation although the vibration is invisible. We employed pulse-width modulated (PWM) current to control the vibration mode of the SMA wire generated from a specially designed amplifier. The control pulse signal has the amplitude of H (V) and a width of W (ms). The duty ratio W/L determines the heating and cooling time of the SMA. $W \times H$, which is equivalent to the calories exchanged during the lengthwise deformation, determines the amplitude of a vibration, and the vibration frequency is completely controlled by regulating L. While generating micro-vibrations of 50 and 100 Hz, a high-speed camera verified that the SMA wire perfectly synchronized with the ON/OFF pulse current and shrunk in the contraction state to approximately 2 μm lengthwise. We confirmed that the vibration frequency was properly controlled up to 400 Hz by the pulse current using our control circuit.

The actuator has an advantage of a compact structure, together with the low energy consumption of approximately 10 mW that enable it to quickly respond to generating vibration. We have also developed a simple structure to amplify the vibration displacement (Zhao et al. 2012). One of the amplification methods is to employ a pin, as shown in Fig. 10.22, which illustrates the structure of the pin-type
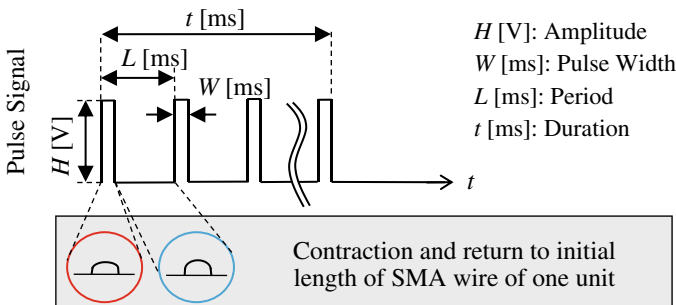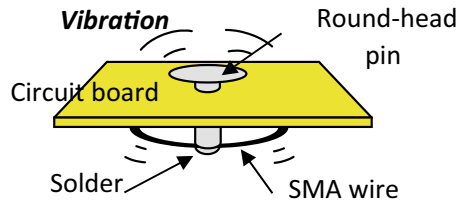

Fig. 10.21 Pulse current for driving SMA actuators

Fig. 10.22 Pin-type actuator

actuator consisting of a 50 µm (diameter) × 3 mm (length) SMA wire and a 1.5 mm (diameter) × 3 mm (length) round head pin. The tip of the pin is soldered at the middle of the SMA wire so that the micro-vibration is efficiently conducted to the pin to be mechanically amplified at the round head.

10.4.4 Application to Tactile Displays

Frequency-controlled vibration generated by the SMA actuators is efficiently applied to present various tactile sensations to human skin. A tactile display is constructed by arranging multiple vibration actuators. Figure 10.23 shows five examples of tactile displays developed in our laboratory, namely (a) tactile mouse, (b) tactile pen, (c) tactile pad, (d) tactile glove, and (e) Braille display. The tactile mouse is equipped with 16 actuators arranged in a 4 × 4 matrix. The 16 actuators are independently driven by the current-control amplifier to present various tactile sensation synchronizing with pictures and movies in a visual display.

a) Tactile mouse   b) Tactile pen   c) Tactile pad

d) Tactile glove   e) Braille display in a mobile phone
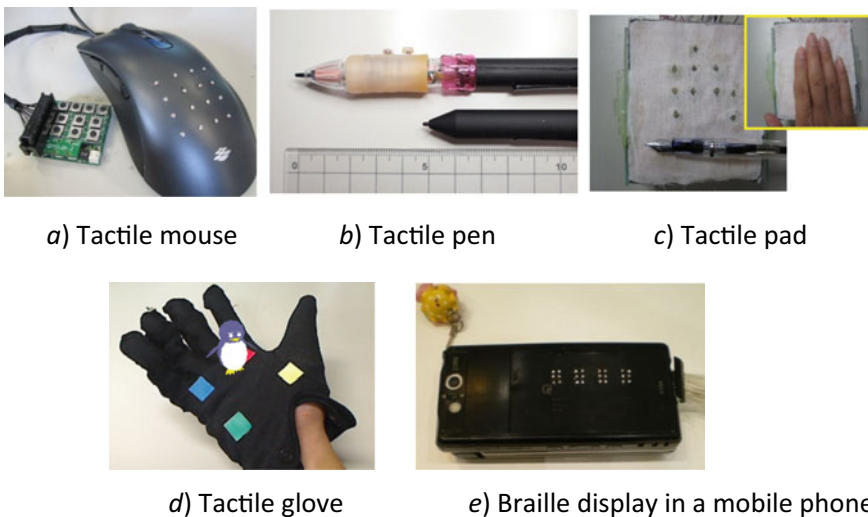
Fig. 10.23 Tactile displays using SMA actuators

Humans feel the texture sensations of an object by touching it with the hand and are also able to imagine the surface textures and tracing sensations from visual information. We tried to extract visual features from a picture by using an image processing technique, and then converted them into pulse signals by selectively determining the frequency, amplitude, and duty ratio (Takeda and Sawada 2013; Jiang et al. 2014). We paid attention to the cyclic patterns included in a picture and tried to relate them with the features of tactile sensations. Cyclic patterns were extracted using Fourier Transform, and parametric values were obtained as the spatial frequency and spectrum amplitude. By relating the spatial frequency with the pulse frequency and the spectral intensity with the duty ratio of a pulse signal, the driving pulse signals for tactile actuators can be automatically generated. In addition, the tactile sensation perceived while stroking an object surface should be changed according to the speed of the hand motion.

In this study, we assumed the following relations among the spectral features of a texture image and the presented tactile sensations:

$$f_p = \alpha(v_p) \cdot g(f_s) \tag{10.42}$$

$$p_w = h(i_s) \tag{10.43}$$

where f_p represents the driving pulse frequency, p_w shows the pulse width, f_s presents the spatial frequency extracted from an input image, i_s represents the spectral intensity of the second peak in a FT image, and v_p presents the speed of a stroking motion on an object. The function α modifies the driving frequency of the actuators according to the speed of the hand motion so that the user perceives the different responses of a tactile sensation reacting to the actions. The functions α, g, and h give the conversion from the image features and user's stroking actions into the driving parameters for the tactile actuators, which are determined by experiments conducted by users.

10.4.5 Application to Fish Robots Having Flexible Bodies

The flexibility of SMA wires are applicable to the bending motion of soft robots (Chen et al. 2020). The authors developed a bionic robotic fish having a soft tail. Two sets of SMA wires were stitched to the two sides of the silicone-fabricated soft tail, allowing the tail to bend on either side, as shown in Fig. 10.24.

The robotic fish body is divided into two parts, a hard body shell in which control systems are installed and the soft silicone tail. The control system includes a control circuit, an infrared transmitter/receiver, and a compact rechargeable lithium battery, and all of them are installed inside the body shell, as shown in Fig. 10.25, to realize an untethered swimming control.

By alternately supplying pulse current to the SMA wires settled in the two sides of the fin, the fin undergoes a flipping motion to propel in water. The swinging motion
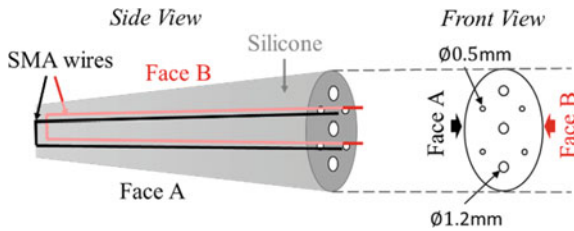
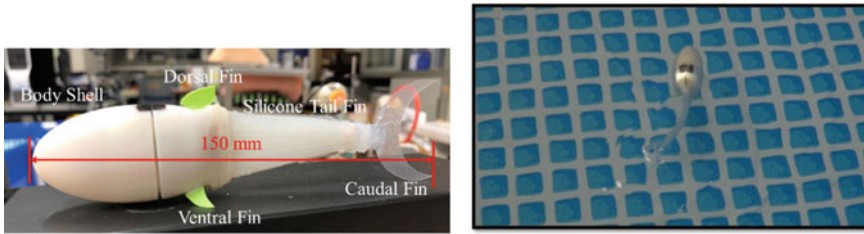**Fig. 10.24** Bionic robotic fish tail using SMA actuators

Fig. 10.25 Untethered bionic fish robot using SMA actuators and its swimming behavior

of the fin is controlled by the frequency of pulse current. For example, a 0.5 Hz fin motion implies slow swimming, while a 3 Hz motion implies swift swimming found in the escaping behavior.

10.4.6 Challenges

In this chapter, novel micro-vibration actuators using shape-memory alloy wires were introduced. As applications, first, the tactile displays consisting of filiform SMA wires with a 50 μm diameter were presented. The display generated micro-vibrations with various frequencies to display various tactile sensation synchronizing with visual and auditory information for VR/AR applications. The actuator features compactness and low energy consumption and is applied to mobile tactile displays and tactile interaction systems by attaching or stitching SMA wires to any surface of a conventional interface device. Second, the application of bionic soft robotic fish was presented. Two SMA wires were installed in the silicone-made fin, and the behavior of bionic fish was successfully realized.

10.5 Bioactuators

10.5.1 Biohybrid Frog-Like Robot

One method for studying the motion of living organisms is to use a biohybrid robot in which a part of the living organism is replaced by a machine. This system is also interesting as an engineering system that directly implements the adaptability of an organism into a machine. In this section, we introduce a bio-muscle-driven frog robot developed by us that implements the muscles of the African clawed frog, which performs excellent swimming locomotion using its legs. Experimental results showed that the frog robot equipped with bioactuators can be driven outside the culture medium.

Movement of living organisms is caused by the interaction between the nervous system, musculoskeletal system, and environment. One method to intervene between these interactions and study their dynamics is to use a biohybrid robot. This method replaces a part of a living body with a machine and investigates changes in its behavior. In this study, we focused on the African clawed frog, Xenopus, which has excellent swimming locomotion, and we created a bio-muscle-driven frog-like robot that realizes the locomotion function of frogs. Frogs have been used in many biohybrid robots that used biological muscles in the past because of their ease of handling, such as the removal of muscles. When biomuscle is driven outside of the culture medium, it has the disadvantage of shorter drive time owing to desiccation and internal ion leakage. Therefore, in previous studies, water tanks were filled with culture medium and the robots were driven inside the tanks. However, this method does not allow the robot to be driven outside of the culture medium, which is a problem that needs to be solved. The authors have developed a bioactuator that packages biomuscle and culture fluid, prevents contact between the biomuscle and the driving environment, and transmits the output of the muscle to the robot.

Various studies have been conducted on the biohybrid robot using frog muscles. Herr et al. extracted semitendinosus muscle from a leopard frog to drive the tail fin structure of a fish-like robot and demonstrated that the muscle could be used as an actuator for the robot by performing swimming motions, such as straight and turning motions (Herr and Dennis 2004). Richards et al. developed robots that can rotate the tibialis posterior muscle of African clawed frogs and swim using servomotors based on the measured output, and they measured the reaction force of water using the sensors on the foot fins (Richards 2011). Using the developed robot, the researchers showed that the thrust force generated by the tibialis posterior muscle varies with the size of the fin, moment arm of the tibialis posterior muscle, and length of the muscle.

Muscle cell actuators are composed of tissue units. Therefore, muscle tissue must be isolated from an individual. The output is large because mature muscle tissue is utilized. However, it is important to conduct the experiment in an ethical manner. The goal is to create an actuator by combining the acquired muscle tissue with the connecting parts of an external mechanical structure. A centimeter-scale myocyte actuator can be obtained, which pulls between two points, and its function is to

Fig. 10.26 Skeletal muscle tissue actuator surrounded by a silicone membrane. The upper figure indicates natural length. The lower figure shows contraction of the actuator

perform a contracting action upon electrical stimulation. Here, leg muscle tissue (tibialis posterior muscle) isolated from an African clawed frog was employed. The completed actuator is shown in Fig. 10.26. Here, the muscle tissue is surrounded by a silicone membrane and closed at both ends. The silicone membrane is filled with saline solution (Ringer's solution) prepared for frogs. Polyethylene threads were sewn onto the tendon portions at both ends of the muscle tissue to connect it to the external mechanical structure. The polyethylene threads have low elongation owing to external force and can efficiently extract displacement. Simultaneously, electrodes were inserted at both ends of the muscle tissue and extracted externally. The build procedure is described as follows:

Step 1: Isolate the tibialis posterior muscle from the leg of the African clawed frog in compliance with ethical standards.

Step 2: Package the muscle tissue. Polyethylene thread is sewn onto the tendon portions at both ends of the muscle tissue. Simultaneously, an electrode (Junflon wire, conductor length: 0.32 mm) is inserted into the muscle. Wrap the electrode in a silicone membrane (Dragonskin 30) and fill the inside with Ringer's solution. Both ends of the membrane are closed.

Step 3: Electrical stimulation is applied to the electrodes (a stimulus group of 7 inputs of square waves of 3.3 V amplitude and 1 ms width at 20 ms intervals, applied at 1000 ms intervals) to drive the robot.

A biohybrid frog-like robot modeled based on an African clawed frog is shown in Fig. 10.27. The body contains an electrical circuit for electrical stimulation of muscles and communication with a PC for remote control. The hind legs reproduce the musculoskeletal system of a frog and are driven by skeletal muscle tissue actuators attached to the legs and thighs. The forelegs are omitted because they do not contribute to the frog's locomotion, such as swimming.

The robot requires a foot structure that mimics the musculoskeletal system of the African clawed frog. The anatomical knowledge and dissected African clawed frogs were used as references for the foot structure. Many of the robot's components
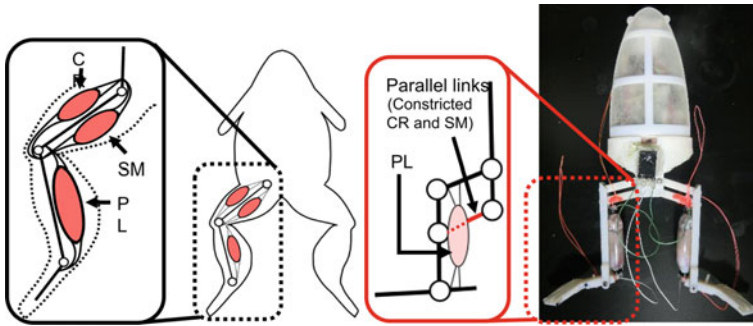
Fig. 10.27 Biohybrid frog-like robot driven by skeletal muscle tissue actuators

are made of Vero White Plus resin printed by a 3D printer (Connex 260TM 3D printing system, Stratasys, Ltd.). Ball bearings are incorporated to reduce friction at each joint. In addition, torsion springs are incorporated in the hip and ankle joints to compensate for the drive of the actuators other than the myocyte actuators. When swimming, the frog extends its legs and scrapes the water with its flippers, thereby increasing the area of its flippers. We reproduced this mechanism. The robot can be divided into three parts: the robot legs driven by biomuscles, the system part consisting of electronic components such as microcontroller, and the exoskeleton part that reproduces the exoskeleton of the frog body. In particular, electronic components including microcontroller and Li–Po batteries are mounted inside the robot.

In the future, we intend to improve the musculoskeletal design of the frog robot, add other muscles to the developed robot, and incorporate sensors and feedback from the environment into the robot, so that the developed frog robot can acquire the motor functions of a frog.

10.5.2 Biohybrid Robot Actuated by Skeletal Muscle Tissues

Skeletal muscle tissue is an attractive bioactuator owing to its strong contractile force, ON/OFF controllability, and dimensional designability. The culture of myoblasts on a device for constructing the tissue allows for the integration of the device and skeletal muscle tissue, enabling the skeletal muscle tissue to be used as an actuator to drive the device. However, simply placing skeletal muscle tissue on a device does not work efficiently. Because the intrinsic traction force, the passive tension, causes a spontaneous shrinkage of the skeletal muscle tissue, leading to malfunction of its contraction, a load of a counter force to the traction force is necessary to prevent shrinkage and maintain the morphology and contractility. There are two main ways to apply a counter force to the skeletal muscle tissue: placement of an antagonistic skeletal muscle tissue and the use of a bendable substrate. The design theory for the device differs depending on the method used.

In biological systems, antagonistic pairs of skeletal muscles are used to overcome shrinkage; the balance of the tension between antagonistic muscles prevents spontaneous shrinkage. By mounting an antagonistic pair of skeletal muscle tissues on a robotic skeleton with a joint similar to that in a biological system, a biohybrid robot can balance the tension between the two tissues. In one study, when selectively applying electrical stimulation to the tissue, joint rotation was achieved, according to the contractions of each tissue. In the robot motion, a large contraction with a strain of the skeletal muscle tissues of 0.2 and joint rotation of 90° was achieved, similar to the motions of the living skeletal muscle and human finger joints (Morimoto et al. 2018) (Fig. 10.28a). Furthermore, the biohybrid robot succeeded in hooking, carrying, and placing a ring by the selective contraction of each skeletal muscle tissue (Fig. 10.28b). Therefore, these results show that the antagonistic pair of skeletal muscle tissues not only prevents shrinkage of the tissue, but can also replicate various finger- and arm-like movements. For the smooth motions, it is important to consider that the configuration of the skeleton influences the robot motion. The motions of the biohybrid robot are determined by the balance between the friction force at the joint and the tensions of skeletal muscle tissues; when this balance does not hold, the joint rotates. It is assumed that the balance can be expressed as follows (Morimoto et al. 2018):

$$F_\mathrm{f} - F_\mathrm{e} \leq \mu(F_\mathrm{f} + F_\mathrm{e} - (2W_\mathrm{a} + W_\mathrm{b})) \tag{10.44}$$

Here, F_f is the tension of the flexor muscle tissue (contracted muscle tissue), F_e is the tension of the extensor muscle (extended muscle tissue), W_a is the weight of the anchor connected to the end of each tissue, W_b is the weight of the bar attached to the joint, and μ is the friction constant at the joint. Because the tension of the skeletal muscle tissue is much larger than the weights of the anchor and bar, they are negligible in the above equation. Therefore, the friction constant is an important factor in determining the magnitude of the joint rotation. In this research, the friction constant at the joint was large (0.46 ± 0.04 (mean $\pm$ s.d., n $=$ 7)); thus, the frictional force imparted resistance to the tension of the tissue, causing a limitation to the joint rotation. Thus, when using skeletal muscle tissue as an actuator, it is important not only to improve its contractility but also to adjust the device characteristics, as smoother joint rotations are possible when the friction constant of the joint is reduced, even if the muscle contractility remains the same. In the case of a bending biohybrid device composed of a flexible sheet and an antagonistic pair of skeletal muscle tissues, the deformation of the sheet can be predicted using a finite element method (FEM) simulation (Morimoto et al. 2019). These results suggest that by understanding the contractility of skeletal muscle tissue and the driving characteristics of the corresponding device, it is possible to design biohybrid robots driven by the tension balance of the antagonistic pair of muscle tissues while predicting the driving style, as in conventional robotics.

Using a bendable substrate, the elastic force of the bent substrate is used as the source of the counter force to the passive tension of the skeletal muscle tissue. The advantage of this method is that it can be driven by a single skeletal muscle tissue. In
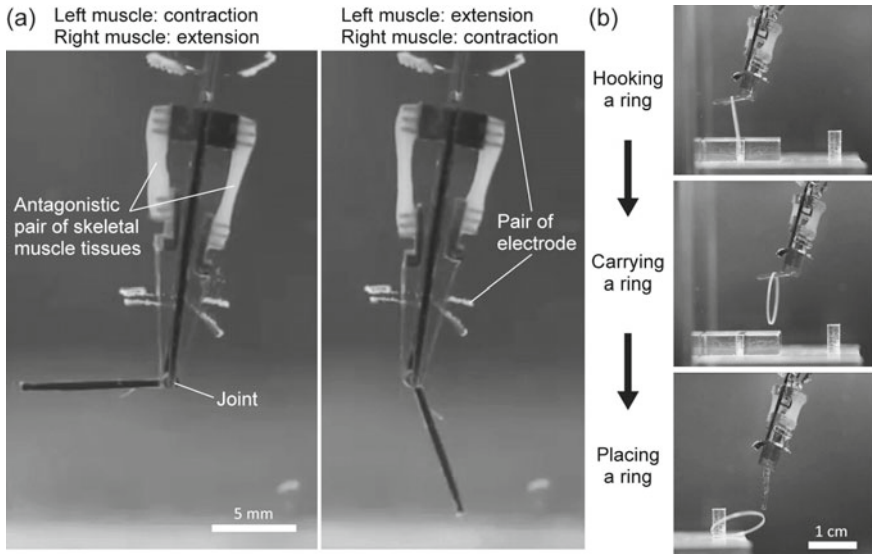
Fig. 10.28 Movements of a biohybrid robot with a joint powered by an antagonistic pair of skeletal muscle tissues. **a** Rotation of the joint according to selective contractions of each skeletal muscle tissue. **b** Manipulation of a ring with the joint rotation—images are reprinted with permission from Morimoto et al. (2018), ©2018, The American Association for the Advancement of Science

addition, by using FEM simulations, it is possible to design a device with appropriate stiffness, i.e., one that does not deform under only the passive tension of the skeletal muscle tissue, but also deforms when its active tension is generated. Although the design of the device must be carefully adjusted to generate a counter force to escape spontaneous muscle shrinkage and malfunctions of the contractility, this method allows for easy tissue construction and electrical stimulation for beginners, as it requires only a single skeletal muscle tissue. In biohybrid robots with a bendable substrate, walking is a typical motion. In the study, when a flexible substrate with two hard pillars was used and the skeletal muscle tissue was bridged between the pillars, its muscle contractions were controlled by the electrical stimulation-induced deformation of the flexible substrate. As a result of the deformation, the locomotion of a biohybrid robot was achieved by kicking the bottom of a culture dish at the tips of the pillars (Cvetkovic et al. 2018; Pagan-Diaz et al. 2018) (Fig. 10.29). Furthermore, by using a method with optogenetically modified skeletal muscle tissues, the robot could walk according to the deformation of its flexible substrate based on light exposure (Raman et al. 2016). As skeletal muscle tissue is made of cells and is vulnerable to desiccation, all of the above biohybrid robots can only work in a culture medium. To overcome this issue, a biohybrid robot with a collagen layer has been proposed. The collagen layer keeps the culture medium inside to prevent the tissue from drying out, even when the robot is in the air. In addition, because flexible electrodes are placed in the collagen layer, the electrical stimuli are transmitted to the skeletal muscle tissue covered with the layer. In one biohybrid robot, deformation of the bendable

substrate and collagen layer was caused by muscle contraction in air (Morimoto et al. 2020) (Fig. 10.30). As a result, the biohybrid robot achieved bending motions in air and successfully accomplished tasks that could not be performed in liquid, such as pushing a bead. The use of skeletal muscle tissue as a driving source is still in its infancy, and further practical applications are expected to emerge in the future.
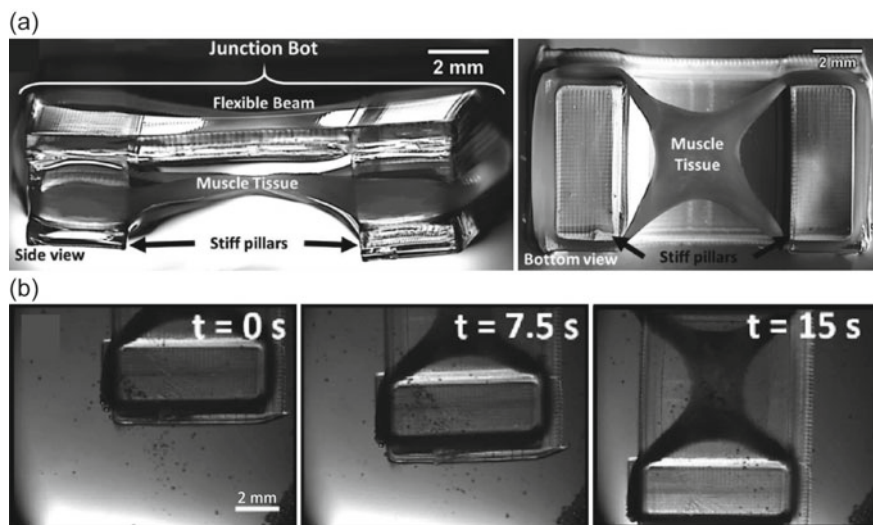

Fig. 10.29 Locomotion of the biohybrid robot on culture dish. **a** Side and bottom view and **b** sequential bottom view of the locomotion—images are reprinted with permission from Pagan-Diaz et al. (2018), ©2018 John Wiley and Sons
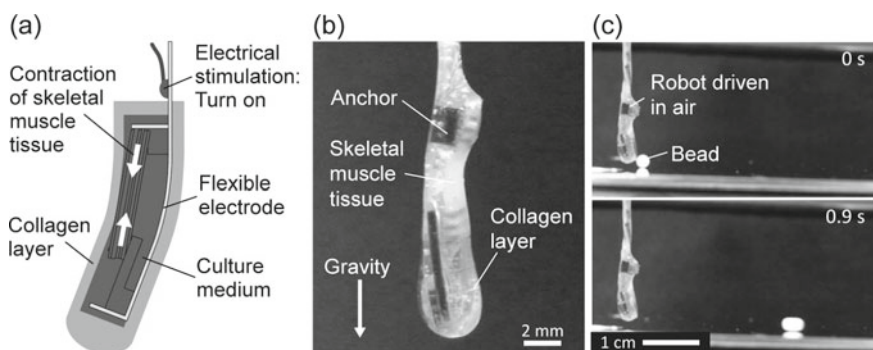

Fig. 10.30 Biohybrid robot driven in air. **a** Conceptual illustration and **b** image of the biohybrid robot covered with a collagen layer. **c** Pushing a bead with the robot—images are reprinted from Morimoto et al. (2020), ©2020 Authors, licensed under a Creative Commons Attribution (CC BY) license

10.5.3 How to Start

To use skeletal muscle tissue as an actuator, it is necessary to prepare equipment for cell culturing and master tissue construction skills. There are many published books and papers on tissue construction, so it is good to refer to them. However, I think the best way is to learn from professors and researchers who specialize in this field, as it requires technical expertise. Meanwhile, as long as the robotic devices are biocompatible and made from materials that do not damage cells, there are no restrictions on how they are fabricated. In addition, at the beginning of research on biohybrid robots with skeletal muscle tissue, I think that it is better to use muscles exploited from living organisms instead of cultured skeletal muscle tissues, so as to check if the robotic device will work with the muscles as desired before starting the work.

10.5.4 Challenges

One of the limitations of using skeletal muscle tissue as an actuator is that the optimal environment is strict, such as a temperature of 37 °C and a pH of approximately 7. Although conventional biohybrid robots have solved this issue by regulating the surrounding environment, it is desirable to be able to adjust these factors internally, such as in living organisms. Therefore, biohybrid robots with such systems will be required in the future.

Exercises

- (8.1) Calculate the ratio of work output and deformation energy W'/E_d in the case where the spring constant of actuator $k_1 = ax_1$ and external load a, $k_2 = $ const. in Fig. 10.4.
- (8.1) Consider the generalized case where the force–displacement relation of the actuator and external load in Fig. 10.4 are $f_1(x)$ and $f_2(x)$, respectively. How does the discussion change?
- (8.2) State the basic motions of fluidic actuators and analyze the possible compositions of basic motions for an octopus' leg.
- (8.2) List the commonly used fabrication techniques for soft fluidic actuators.
- (8.2) Specify the types of fluidic pressure sources and compare the pros and cons of each pressure source.
- (8.3) What are the parameters to derive the Maxwell stress?
- (8.3) What is the role of cations in IPMCs?
- (8.3) Discuss the best application for DEAs and IPMCs.
- (8.4) Considering the physical properties of shape-memory alloy actuators, propose possible applications for the actuation of robots.
- (8.4) By applying the pseudoelasticity of shape-memory alloys, propose a new force-sensing method or a device applicable to robots.

- (8.5) What methods are mainly used to load the counter force to the passive tension of the skeletal muscle tissue?

References

Acome E, Mitchell SK, Morrissey TG, Emmett MB, Benjamin C, King M, Radakovitz M, Keplinger C (2018) Hydraulically amplified self-healing electrostatic actuators with muscle-like performance. Science 359:61–65

Anderson IA, Gisby TA, McKay TG et al (2012) Multi-functional dielectric elastomer artificial muscles for soft and smart machines. J Appl Phys 112:041101. https://doi.org/10.1063/1.4740023

Asaka K, Oguro K, Nishimura Y et al (1995) Bending of polyelectrolyte membrane–platinum composites by electric stimuli I. Response characteristics to various waveforms. Polym J 27:436–440. https://doi.org/10.1295/polymj.27.436

Aubin CA, Choudhury S, Jerch R, Archer LA, Pikul JH, Shepherd RF (2019) Electrolytic vascular systems for energy-dense robots. Nature 571(7763):51–57

Bar-Cohen Y (2004) Electroactive polymer (EAP) actuators as artificial muscles: reality, potential, and challenges, 2nd edn. SPIE, Bellingham, WA

Bar-Cohen Y, Xue T, Shahinpoor M et al (1998) Flexible, low-mass robotic arm actuated by electroactive polymers and operated equivalently to human arm and hand. In: Robotics 98. American Society of Civil Engineers, Reston, VA, pp 15–21

Bellini A, Colli M, Dragoni E (2009) Mechatronic design of a shape memory alloy actuator for automotive tumble flaps: a case study. IEEE Trans Ind Electron 56(7):2644–2656

Brochu P, Pei Q (2010) Advances in dielectric elastomers for actuators and artificial muscles. Macromol Rapid Commun 31:10–36. https://doi.org/10.1002/marc.200900425

Cacucciolo V, Shintake J, Kuwajima Y, Maeda S, Floreano D, Shea H (2019) Stretchable pumps for soft machines. Nature 572(7770):516–519

Carpi F (2016) Electromechanically active polymers. Springer International Publishing, Cham

Chen X, Shigemune H, Sawada H (2020) An untethered bionic robotic fish using SMA actuators. In: Proceedings of IEEE international conference on mechatronics and automation (IEEE ICMA2020), pp 1768–1773

Cohen YB (2004) Electroactive polymer (EAP) actuators as artificial muscles: reality, potential, and challenges. SPIE Press

Constantin P, Foias C (1988) Navier-stokes equations. University of Chicago Press

Cvetkovic C, Raman R, Chan V, Williams BJ, Tolish M, Bajaj P, Sakar MS, Asada HH, Saif MTA, Bashir R (2018) Three-dimensionally printed biological machines powered by skeletal muscle. Proc Natl Acad Sci USA 111(28):10125–10130

Danjo J, Danjo S, Nakamura Y, Uchida K, Sawada H (2016) Micro-vibration patterns generated from shape memory alloy actuators and the detection of an asymptomatic tactile sensation decrease in diabetic patients. IEICE Trans Inf Syst E99-D(11):2759–2766

Danjo J, Sawada H, Uchida K, Danjo S, Nakamura Y (2017) Efficacy of a new microvibration sensation measurement device at detecting diabetic peripheral neuropathy using a newly devised finger method. J Gen Fam Med 18(4):155–161

Diteesawat RS, Helps T, Taghavi M, Rossiter J (2021) Electro-pneumatic pumps for soft robotics. Sci Robot 6(51)

Elger DF, LeBret BA, Crowe CT, Roberson JA (2020) Engineering fluid mechanics. Wiley

Fukui Y, Inamura T, Hosoda H, Wakashima K, Miyazaki S (2004) Mechanical properties of a Ti–Nb–Al shape memory alloy. Mater Trans 45(4):1077–1082

Garrad M, Soter G, Conn AT, Hauser H, Rossiter J (2019) Driving soft robots with low-boiling point fluids. In: IEEE international conference on soft robotics, pp 74–79

Geier A, Tucker RCY, Somlor S, Sawada H, Sugano S (2020) End-to-end tactile feedback loop: from soft sensor skin over deep GRU-autoencoders to tactile stimulation. IEEE Robot Autom Lett 5(4):6467–6474. https://doi.org/10.1109/LRA.2020.3012951

Gorissen B, Reynaerts D, Konishi S, Yoshida K, Kim JW, De Volder M (2017) Elastic inflatable actuators for soft robotic applications. Adv Mater 29(43):1604977

Gu G-Y, Zhu J, Zhu L-M, Zhu X (2017) A survey on dielectric elastomer actuators for soft robots. Bioinspir Biomim 12:011003. https://doi.org/10.1088/1748-3190/12/1/011003

Guo Y, Liu L, Liu Y, Leng J (2021) Review of dielectric elastomer actuators and their applications in soft robots. Adv Intell Syst 3:2000282. https://doi.org/10.1002/aisy.202000282

Hafiz M, Sawada H (2011) Presentation of button repulsive sensations on touch screen using SMA wires. In: IEEE international conference on mechatronics and automation, pp 1–6

Haines CS, Márcio DL, Li N, Spinks GM, Foroughi J, Madden JDW, Kim SH, Fang S, Andrade MJD, Göktepe F, Göktepe Ö, Mirvakili SM, Naficy S, Lepró X, Oh J, Kozlov ME, Kim SJ, Xu X, Swedlove BJ, Wallace GG, Baughman RH (2014) Artificial muscles from fishing line and sewing thread. Science 343:868–872

Herr H, Dennis RG (2004) A swimming robot actuated by living muscle tissue. J Neuroeng Rehabil 1(1):6

Higuchi T, Suzumori K, Tadokoro S (eds) (2009) Next-generation actuators leading breakthroughs. Springer

Hiramitsu T, Suzumori K, Nabae H, Endo G (2019) Experimental evaluation of textile mechanisms made of artificial muscles. In: IEEE international conference on soft robotics (RoboSoft). IEEE, pp 1–6

Horiuchi T, Mihashi T, Fujikado T et al (2017) Voltage-controlled IPMC actuators for accommodating intra-ocular lens systems. Smart Mater Struct 26:045021. https://doi.org/10.1088/1361-665X/aa61e8

Huang J, Shian S, Diebold RM et al (2012) The thickness and stretch dependence of the electrical breakdown strength of an acrylic dielectric elastomer. Appl Phys Lett 101:122905. https://doi.org/10.1063/1.4754549

Huber JE, Fleck NA, Ashby MF (1997) The selection of mechanical actuators based on performance indices. Proc R Soc Lond A 453:2185–2205

Ji X, El Haitami A, Sorba F et al (2018) Stretchable composite monolayer electrodes for low voltage dielectric elastomer actuators. Sens Actuators B Chem 261:135–143. https://doi.org/10.1016/j.snb.2018.01.145

Ji X, Liu X, Cacucciolo V, Imboden M, Civet Y, Haitam AE, Cantin S, Perriard Y, Shea H (2019) An autonomous untethered fast soft robotic insect driven by low-voltage dielectric elastomer actuators. Sci Robot 4:eaaz6451

Jiang C, Uchida K, Sawada H (2014) Research and development of vison based tactile display system using shape memory alloys. Int J Innov Comput Inf Control 10(3):837–850

Juan JS, No ML, Schuh CA (2008) Superelasticity and shape memory in micro- and nanometer-scale pillars. Adv Mater 20(2):272–278

Kanno R, Nagai T, Shintake J (2021) Rapid fabrication method for soft devices using off-the-shelf conductive and dielectric acrylic elastomers. Adv Intell Syst 3:2000173. https://doi.org/10.1002/aisy.202000173

Katzschmann RK, DelPreto J, MacCurdy R, Rus D (2018) Exploration of underwater life with an acoustically controlled soft robotic fish. Sci Robot 3(16)

Kennedy DK, Straub FK, Schetky LMD, Chaudhry Z, Roznoy R (2004) Development of an SMA actuator for in-flight rotor blade tracking. J Intell Mater Syst Struct 15(4):235–248

Kim B, Lee MG, Lee YP, Kim Y, Lee G (2006) An earthworm-like micro robot using shape memory alloy actuator. Sens Actuators A Phys 125(2):429–437

Kitamori T, Wada A, Nabae H, Suzumori K (2016) Untethered three-arm pneumatic robot using hose-free pneumatic actuator. In: 2016 IEEE/RSJ international conference on intelligent robots and systems (IROS). IEEE, pp 543–548

Kodaira A, Asaka K, Horiuchi T, Endo G, Nabae H, Suzumori K (2019) IPMC monolithic thin film robots fabricated through a multi-layer casting process. IEEE Robot Autom Lett 4:1335–1342

Kurumaya S, Suzumori K, Nabae H, Wakimoto S (2016) Musculoskeletal lower-limb robot driven by multifilament muscles. Robomech J 3(1):1–15

Li Y, Hashimoto M (2016) Design and prototyping of a novel lightweight walking assist wear using PVC gel soft actuators. Sens Actuators A Phys 239:26–44

Mao Z, Iizuka T, Maeda S (2021) Bidirectional electrohydrodynamic pump with high symmetrical performance and its application to a tube actuator. Sens Actuators A Phys 332:113168

Melton KN, Mercier O (1981) The mechanical properties of NiTi-based shape memory alloys. Acta Metall 29(2):393–398

Mirvakili SM, Hunter IW (2018) Artificial muscles: mechanisms, applications, and challenges. Adv Mater 30:1704407. https://doi.org/10.1002/adma.201704407

Mizukami Y, Sawada H (2006) Tactile information transmission by apparent movement phenomenon using shape-memory alloy device. Int J Disabil Hum Dev 5(3):277–284

Morimoto Y, Onoe H, Takeuchi S (2018) Biohybrid robot powered by an antagonistic pair of skeletal muscle tissues. Sci Robot 3(18):eaat4440

Morimoto Y, Onoe H, Takeuchi S (2019) Biohybrid device with antagonistic skeletal muscle tissues for measurement of contractile force. Adv Robot 33(5):208–218

Morimoto Y, Onoe H, Takeuchi S (2020) Biohybrid robot with skeletal muscle tissue covered with a collagen structure for moving in air. APL Bioeng 4(2):026101

Morin SA, Kwok SW, Lessing J, Ting J, Shepherd RF, Stokes AA, Whitesides GM (2014) Elastomeric tiles for the fabrication of inflatable structures. Adv Funct Mater 24(35):5541–5549

Nabae H, Kodaira A, Horiuchi T et al (2019) Soft polymer-electrolyte-fuel-cell tube realizing air-hose-free thin McKibben muscles. In: 2019 IEEE/RSJ international conference on intelligent robots and systems (IROS). IEEE, pp 8287–8293

Onal CD, Chen X, Whitesides GM, Rus D (2017) Soft mobile robots with on-board chemical pressure generation. In: Robotics research. Springer, Cham, pp 525–540

Pagan-Diaz GJ, Zhang XT, Grant L, Kim Y, Aydin O, Cvetkovic C, Ko E, Solomon E, Hollis J, Kong H, Saif T, Gazzola M, Bashir R (2018) Simulation and fabrication of stronger, larger, and faster walking biohybrid machines. Adv Funct Mater 28(23):1801145

Pan Q, Cho C (2007) The investigation of a shape memory alloy micro-damper for MEMS applications. Sensors 7(9):1887–1900

Park I-S, Jung K, Kim D et al (2008) Physical principles of ionic polymer–metal composites as electroactive actuators and sensors. MRS Bull 33:190–195. https://doi.org/10.1557/mrs2008.44

Peele BN, Wallin TJ, Zhao H, Shepherd RF (2015) 3D printing antagonistic systems of artificial muscle using projection stereolithography. Bioinspir Biomim 10(5):055003

Pelrine RE, Kornbluh RD, Joseph JP (1998) Electrostriction of polymer dielectrics with compliant electrodes as a means of actuation. Sens Actuators A Phys 64:77–85. https://doi.org/10.1016/S0924-4247(97)01657-9

Piao M, Miyazaki S, Otsuka K (1992) Characteristics of deformation and transformation in $Ti_{44}Ni_{47}Nb_9$ shape memory alloy. Mater Trans JIM 33(4):346–353

Polygerinos P, Correll N, Morin SA, Mosadegh B, Onal CD, Petersen K, Cianchetti MT, Michael T, Shepherd RF (2017) Soft robotics: review of fluid-driven intrinsically soft devices; manufacturing, sensing, control, and applications in human-robot interaction. Adv Eng Mater 19(12):1700016

Raman R, Cvetkovic C, Uzel SGM, Platt RJ, Sengupta P, Kamm RD, Bashir R (2016) Optogenetic skeletal muscle-powered adaptive biological machines. Proc Natl Acad Sci USA 113(13):3497–3502

Reynaerts D, Peirs J, Brussel HV (1999) Shape memory micro-actuation for a gastro-intestinal intervention system. Sens Actuators A Phys 77(2):157–166

Richards CT (2011) Building a robotic link between muscle dynamics and hydro-dynamics. J Exp Biol 214(14):2381–2389

Robinson SS, O'Brien KW, Zhao H, Peele BN, Larson CM, Mac Murray BC, Shepherd RF (2015) Integrated soft sensors and elastomeric actuators for tactile machines with kinesthetic sense. Extreme Mech Lett 5:47–53

Rosset S, Shea HR (2016) Small, fast, and tough: shrinking down integrated elastomer transducers. Appl Phys Rev 3:031105. https://doi.org/10.1063/1.4963164

Shahinpoor M (2020) Fundamentals of smart materials. Royal Society of Chemistry

Shepherd RF, Ilievski F, Choi W, Morin SA, Stokes AA, Mazzeo AD, Whitesides GM (2011) Multigait soft robot. Proc Natl Acad Sci 108(51):20400–20403

Shintake J, Rosset S, Schubert BE et al (2015) A foldable antagonistic actuator. IEEE/ASME Trans Mechatron 20:1997–2008. https://doi.org/10.1109/TMECH.2014.2359337

Shintake J, Rosset S, Schubert B et al (2016) Versatile soft grippers with intrinsic electroadhesion based on multifunctional polymer actuators. Adv Mater 28:231–238. https://doi.org/10.1002/adma.201504264

Shintake J, Cacucciolo V, Floreano D, Shea H (2018a) Soft robotic grippers. Adv Mater 30. https://doi.org/10.1002/adma.201707035

Shintake J, Cacucciolo V, Shea H, Floreano D (2018b) Soft biomimetic fish robot made of dielectric elastomer actuators. Soft Robot 5:466–474. https://doi.org/10.1089/soro.2017.0062

Singh K, Sirohi J, Chopra I (2003) An improved shape memory alloy actuator for rotor blade tracking. J Intell Mater Syst Struct 14(12):767–786

Stratton JA (2007) Electromagnetic theory. Wiley

Sun F, Hao YL, Nowak S, Gloriant T, Laheurte P, Prima F (2011) A thermo-mechanical treatment to improve the superelastic performances of biomedical Ti–26Nb and Ti–20Nb–6Zr (at.%) alloys. J Mech Behav Biomed Mater 4(8):1864–1872

Suzumori K, Iikura S, Tanaka H (1992) Applying a flexible microactuator to robotic mechanisms. IEEE Control Syst Mag 12(1):21–27

Suzumori K, Wada A, Wakimoto S (2013) New mobile pressure control system for pneumatic actuators, using reversible chemical reactions of water. Sens Actuators A Phys 201:148–153

Takagi K, Yamamura M, Luo Z et al (2006) Development of a rajiform swimming robot using ionic polymer artificial muscles. In: 2006 IEEE/RSJ international conference on intelligent robots and systems. IEEE, pp 1861–1866

Takeda Y, Sawada H (2013) Tactile actuators using SMA micro-wires and the generation of texture sensation from images. In: IEEE/RSJ international conference on intelligent robots and systems (IROS2013), pp 2017–2022

Tolley MT, Shepherd RF, Karpelson M, Bartlett NW, Galloway KC, Wehner M, Wood RJ (2014) An untethered jumping soft robot. In: IEEE/RSJ international conference on intelligent robots and systems, pp 561–566

Tse YA, Wong KW, Yang Y, Wang MY (2020) Novel design of a soft pump driven by super-coiled polymer artificial muscles. In: IEEE/RSJ international conference on intelligent robots and systems (IROS), pp 8789–8794

Wang N, Cui C, Guo H et al (2018) Advances in dielectric elastomer actuation technology. Sci China Technol Sci 61:1512–1527. https://doi.org/10.1007/s11431-017-9140-0

Wehner M, Truby RL, Fitzgerald DJ, Mosadegh B, Whitesides GM, Lewis JA, Wood RJ (2016) An integrated design and fabrication strategy for entirely soft, autonomous robots. Nature 536(7617):451–455

Xu B, Hu M, Zhang JH, Mao ZB (2017) Distribution characteristics and impact on pump's efficiency of hydro-mechanical losses of axial piston pump over wide operating ranges. J Cent South Univ 24(3):609–624

Yeghiazarian L, Mahajan S, Montemagno C, Cohen C, Wiesner U (2005) Directed motion and cargo transport through propagation of polymer-gel volume phase transitions. Adv Mater 17:1869–1873
Zhao F, Jiang C, Sawada H (2012) A novel Braille display using the vibration of SMA wires and the evaluation of Braille presentations. J Biomech Sci Eng 7(4):416–432